Dehydration and partial melting in subduction zones: Constraints from U-series disequilibria

Bernard Bourdon, Simon Turner, Anthony Dosseto

JOURNAL OF GEOPHYSICAL RESEARCH, VOL. 108, NO. B6, 2291, doi:10.1029/2002JB001839, 2003

Dehydration and partial melting in subduction zones: Constraints from U-series disequilibria

Bernard Bourdon
Laboratoire de Géochimie et Cosmochimie, IPGP-CNRS, Paris cedex, France

Simon Turner
Department of Earth Sciences, University of Bristol, Bristol, UK

Anthony Dosseto
Laboratoire de Géochimie et Cosmochimie, IPGP-CNRS, Paris cedex, France

Received 22 February 2002; revised 22 January 2003; accepted 11 February 2003; published 6 June 2003.

[1] We present a critical reappraisal of U-series data from arc volcanoes to constrain slab dehydration and melting processes using a global subduction zone data set. There is no clear evidence for significant mobilization of Th or Pa in dehydration fluids while the source region of arc rocks is relatively oxidized and mobility of U is strongly enhanced. It is argued that along-arc U/Th and U/Pa isotope data reflect time-integrated addition of U from the slab to the mantle wedge. The presence of large Ra-Th disequilibrium correlated with Ba/Th ratios provides evidence for some very recent fluid addition and fast magma ascent. This is consistent with radiogenic Os isotope signatures in arc lavas that can only be preserved if there is no melt-peridotite equilibration during melt transport. The ^{231}Pa excesses found in most arc lavas provide clear evidence for a melting signature and require that the timescale of melt production cannot be as short as the timescale of melt migration (<100 annum). We propose a dynamic model in which melting is initiated by fluid fluxing and where melt is rapidly extracted out of the mantle via high-velocity channels while ^{231}Pa excess is produced at melting rates consistent with literature estimates of melt productivity. An alternative model with continuous flux melting would require a long melting timescale (1–5 Ma), a large melting region and the mobility of Th and Pa in fluids. A model with a time lag between melting and initial dehydration is more consistent with a thermal structure where the wet solidus is not reached before an intermediate depth. *INDEX TERMS:* 1040 Geochemistry: Isotopic composition/chemistry; 3640 Mineralogy, Petrology, and Mineral Physics: Igneous petrology; 8434 Volcanology: Magma migration; 8450 Volcanology: Planetary volcanism (5480); *KEYWORDS:* subduction zone, melting, dehydration, U-series, timescale

Citation: Bourdon, B., S. Turner, and A. Dosseto, Dehydration and partial melting in subduction zones: Constraints from U-series disequilibria, *J. Geophys. Res.*, *108*(B6), 2291, doi:10.1029/2002JB001839, 2003.

1. Introduction

[2] Subduction zones and mid-ocean ridges are the two key sites of generation of the Earth's magmatism and plate driving forces. However, whereas mid-ocean ridges do not return material from the crust to the mantle, subduction zones play a pivotal role in the long-term compositional evolution of the mantle-crust system. The role of subduction zones in global geochemical dynamics is thus twofold: first, crustal material with a radically distinct geochemical signature is recycled back into the deep mantle, and second, there is production of material with affinities to the continental crust. Many studies have now documented that subduction zone lavas carry contributions from several components including the mantle wedge, the recycled oceanic crust, subducted sediments, and in some cases the continental crust underlying the arc. These have enabled the estimation of the relative crust to mantle and mantle to crust fluxes [e.g., *Hawkesworth et al.*, 1991; *Plank and Langmuir*, 1998; *Elliott et al.*, 1997; *Turner et al.*, 1997a, 1997b]. However, in this paper, we examine subduction zones from the perspective that while partial melting beneath ridges is well modeled as the response to decompression, the primary controls on melting at subduction zones remain surprisingly poorly understood. In particular, there has been considerable debate as to whether partial melting primarily reflects lowering of the peridotite solidus by addition of aqueous fluids from the subducting oceanic crust, whether the degree of melting varies with the size of the fluid flux, and whether there is additionally a component of decompression melting, despite the confines of the mantle wedge. Our aim is to

0148-0227/03/2002JB001839$09.00

develop a better understanding of the melting process by constraining the relative rates and timescales of dehydration fluid addition and decompression melting. Most of these constraints derive from recent studies of U-series disequilibria, and so after a brief synthesis of available geophysical and geochemical constraints, we review the U-series data and take a critical look at some of the debates surrounding their interpretation. Finally, we combine these with the pertinent geophysical data to develop an integrated model for partial melting at subduction zones.

2. Geophysical and Geochemical Constraints on Dehydration and Melting Beneath Arc Volcanoes

[3] Understanding the processes of partial melting at subduction zones has been a long-standing goal of the Earth sciences and some consensus has started to emerge over the past few decades concerning processes which are ''unlikely'' to be important. For example, it has been shown that friction on the upper surface of the slab is insufficient to generate enough heat to initiate melting [*Molnar and England*, 1995]. Similarly, modeling of geothermal structure at the slab-wedge interface has shown that melting of the slab itself is likely to occur only when the slab is very young [*Peacock et al.*, 1994]. More generally, it has been concluded that the release of fluids from the slab metasomatizes the overlying mantle wedge which undergoes melting as it crosses its wet solidus due to entrainment by the downgoing slab [*Tatsumi*, 1989]. The study of metamorphic reactions in the basalt-H_2O system has shown that the release of fluids from the slab takes place over an extended range of depths [*Schmidt and Poli*, 1998], such that the relatively constant depth to the Wadati-Benioff found by *Gill* [1981] cannot be attributed to a single dehydration reaction. As we discuss below, this is consistent with recent models in which the onset of partial melting is governed by an isotherm [*England*, 2001] corresponding to the wet peridotite solidus rather than the pressure of a particular dehydration reaction.

[4] Thermal modeling of subduction zones has suggested that melting is likely to take place only in the hot core of the mantle wedge where temperatures exceed 1000°C [*Davies and Stevenson*, 1992; *Kincaid and Selwyn Sacks*, 1997; *Peacock*, 1990; *Iwamori*, 1998]. There are, however, large uncertainties about the thermal structure of the mantle wedge, particularly near the slab-wedge interface. The relative velocity of entrained wedge and subducting slab is crucial for determining this thermal structure and reflects the degree of coupling between the two, yet the presence of fluids will lead to reductions in viscosity which could, in turn, reduce this coupling. Additional complexity comes from the suggestions [*Marsh*, 1979; *Plank and Langmuir*, 1988; *Pearce and Parkinson*, 1993; *Brémont d'Ars et al.*, 1995; *Spiegelman and McKenzie*, 1987; *Furukawa*, 1993] that upwelling occurs beneath the arc volcanoes and this should also depend on the extent to which the mantle overlying the slab is hydrated. The along-arc dimension is crucial for determining buoyancy within the wedge and a simple observation in support of a 3-D, rather than a 2-D, structure is the spacing of arc volcanoes [*Brémont d'Ars et al.*, 1995].

[5] In a complementary way, interpretations arising from geochemical and petrological investigations also impinge upon models for the nature of mantle wedge circulation, and it has become a nontrivial exercise to try and integrate all the information provided by the various tracers for melting and dehydration [*Elliott et al.*, 1997]. For example, numerous studies have suggested that the transfer of the sediment component from the subducted slab into the wedge occurs as a partial melt rather than bulk addition [e.g., *Elliott et al.*, 1997; *Turner et al.*, 1997a, 1997b]. Yet most current thermal models predict temperatures at the slab-wedge interface which are too low for sediment melting and the predicted temperature at the slab interface will be even cooler if there is decoupling between the wedge and slab motions, as recently suggested for the Tonga arc [*Turner and Hawkesworth*, 1997, 1998; *Smith et al.*, 2001]. The depth of melt generation within the mantle wedge is also poorly constrained. Rare earth element (REE) data generally suggest that melting takes place in the spinel lherzolite field but if the melting region can be approximated by a 1-D column, the REE data could merely reflect the depth of last equilibration [*Dosseto et al.*, 2003; *Pearce and Parkinson*, 1993]. It is also not clear how the addition of fluids controls the degree of melting. If melt is rapidly extracted from the mantle source, the lowering of the peridotite solidus [*Hirose and Kawamoto*, 1995] becomes ineffective because water, being a highly incompatible element, is removed in the first melt fractions leaving the residual peridotite unproductive unless it attains the temperature of the dry solidus. However, if the melt interacts with the matrix, then the extent of melting will be controlled by the wet solidus [*Hirschmann et al.*, 1999]. Finally, the extent of melt-peridotite interaction and the depth of last equilibration are only poorly constrained by modeling of major and trace element data [*Kelemen et al.*, 1990], yet the extent of melting could be deeply modified by the melt migration and equilibration process.

3. U-Series Systematics in Subduction Zone Lavas

[6] The available U-series isotope data from subduction zones are shown in Figure 1 and come largely from the ^{238}U-^{230}Th (^{230}Th half-life 75 ka), ^{235}U-^{231}Pa (^{231}Pa half-life 32 ka), and ^{226}Ra-^{230}Th (^{226}Ra half-life 1.6 ka) systems, which record parent-daughter fractionation occurring on timescales on the order of the daughter half-lives indicated. Thus an activity ratio deviating from one indicates a recent elemental fractionation that can be attributed to melting or fluid addition. We review each parent-daughter system, in turn, discussing the various interpretations proposed in the literature and highlighting the extent to which these interpretations are consistent or inconsistent with the other systems. Throughout this paper, activity ratios ($\lambda_1 N_1/\lambda_2 N_2$, where λ_i and N_i are the decay constants and number of atoms, respectively) are used instead of atomic ratios for U-series nuclides.

3.1. $^{238}U/^{230}Th$ Systematics

[7] There are more data for the ^{238}U-^{230}Th system than for either of the other pairs considered here and since the first studies by *Allègre and Condomines* [1982], it has been shown that most arc lavas are characterized by ^{238}U excess relative to ^{230}Th (i.e., an activity ratio $^{238}U/^{230}Th$ greater

than one) (Figure 1a). Because U is fluid-mobile under oxidizing conditions (as U^{6+}), the ^{238}U excesses have been interpreted to reflect the addition of U by fluids released from the downgoing slab. This interpretation relies heavily on the assumption that the source of fluids is oxidized enough for uranium to be mostly in the U^{6+} state. There is indeed ample evidence that arc lavas and peridotite from the subarc mantle are more oxidized. Arc lavas display oxygen fugacities + 2 units above the Fayalite-magnetite-quartz (FMQ) buffer while arc peridotites show oxygen fugacities + 1 to + 2 units above FMQ [*Balhaus et al.*, 1990; *Parkinson and Arculus*, 1999]. For this range of f_{o2}, it has been shown experimentally that U partitions into fluid preferentially over Th [*Brenan et al.*, 1996]. Moreover, because Th remains in the 4 + state, it will be much less mobile in aqueous fluids than U and so the simplest model for addition of fluids to the mantle wedge produces a horizontal array on the ^{230}Th-^{238}U isochron diagram (see inset to Figure 1a). Like ocean island and mid-ocean ridge basalts (OIB and MORB), the lavas from subduction zones rarely form well-defined trends, however, several subduction zones (Marianas, Vanuatu, Tonga-Kermadec) are characterized by crude, positively sloped linear trends in Figure 1a. In the simplest model, these sloped arrays represent the along-arc, time-integrated ^{230}Th in-growth between fluid addition and eruption over which the array rotates back toward the equiline. It is important to recognize that this interpretation is only valid if (1) shallow-level processes do not perturb U-series systematics, (2) the fluid added to the mantle wedge contains negligible amounts of Th, (3) the $^{230}Th/^{232}Th$ isotope composition of the mantle wedge was the same for all of the lavas prior to fluid addition, and (4) the effects of partial melting do not subsequently disturb the U-Th isotope systematics. As we discuss below, all of these assumptions have been challenged.

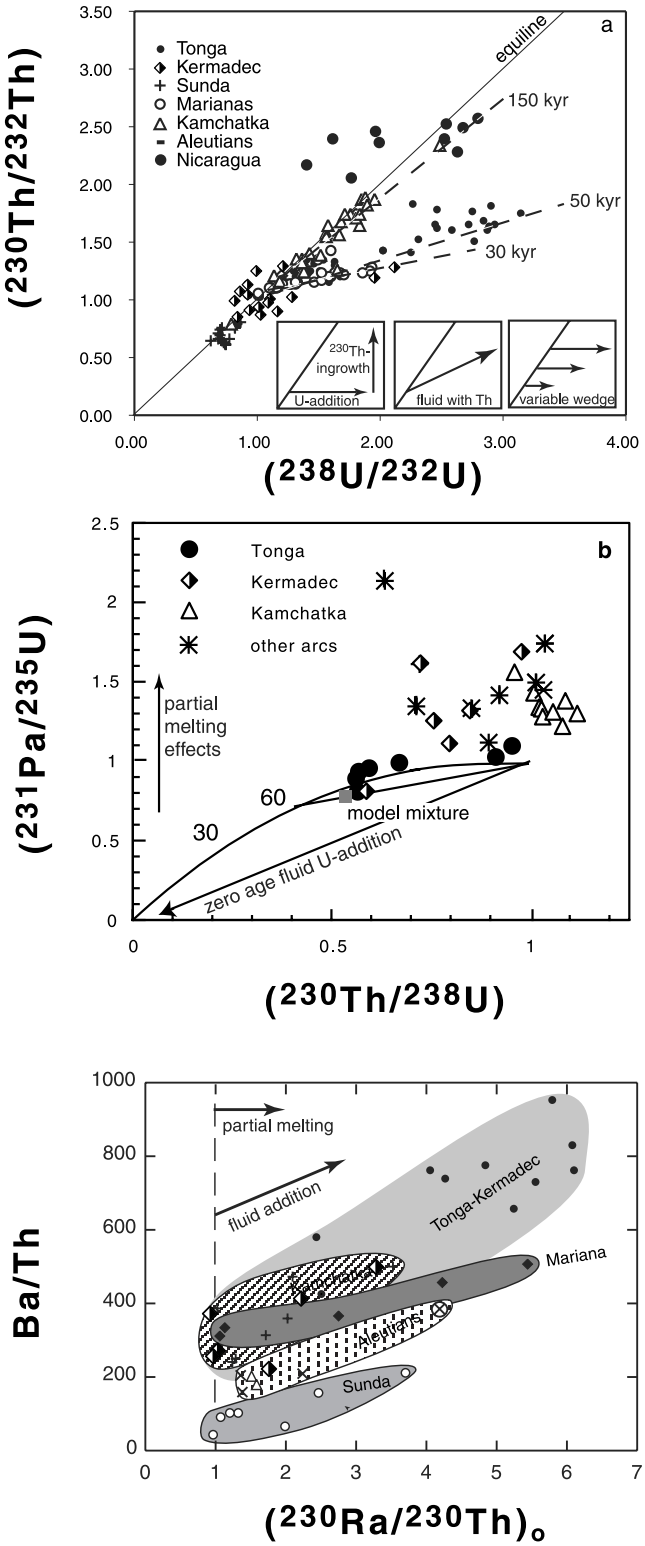

3.2. $^{235}U/^{231}Pa$ Systematics

[8] Pa, which is characterized by a + 5 charge behaves as a high-field strength element and is unlikely to be fluid mobile relative to U, therefore the simplest model predicts that subduction zone lavas will have excesses of ^{235}U over ^{231}Pa. Consequently, the discovery by *Pickett and Murrell* [1997] that most subduction zone lavas in fact have ^{231}Pa excesses similar to MORB and OIB was unexpected and suggested that the effects of partial melting are to produce increases in ^{231}Pa which overprint the effects of U addition by fluids (see Figure 1b). The only lavas to have excesses of ^{235}U over ^{231}Pa are those from Tonga (Figure 1b) where partial melting is unlikely to fractionate Pa/U ratios because the highly depleted nature of the mantle wedge results in a low mode of residual clinopyroxene during melting [*Bourdon et al.*, 1999]. By normalizing Pa to Nb, *Bourdon et al.* [1999] showed that the Pa-U disequilibria in the Tonga arc

Figure 1. (opposite) (a) Compilation of mass spectrometric measurements of U-series disequilibria in subduction zone lavas. (a) ^{238}U-^{230}Th isochron diagram on which most subduction zones show inclined arrays (corresponding age indicated). (b) ($^{231}Pa/^{235}U$) versus ($^{230}Th/^{238}U$) diagram. The concordia line represents the composition of a fluid evolving with no initial ^{230}Th or ^{231}Pa. A mixture of a 60-ka-old fluid with a depleted mantle wedge is shown by the straight solid line. The gray square represents a mixture of a depleted mantle wedge with 2% fluid. (c) $(^{226}Ra/^{230}Th)_0$ versus Ba/Th ratios. $(^{226}Ra/^{230}Th)_0$ activity ratios were corrected for decay since eruption. Data from *Bourdon et al.* [1999], *Dosseto et al.* [2003], *Elliott et al.* [1997], *Gill et al.* [1993], *Reagan et al.* [1994], *Turner and Foden* [2001], and *Turner et al.* [1997a, 1997b, 1998, 2000, 2001].

yields a pseudoage (60 ka) which is strikingly similar to the 50-ka age estimated from the U-Th disequilibria [*Turner et al.*, 1997a, 1997b]. The concordance from two independent systems argues, as strongly as anything else, that the slopes of the U-Th arrays on Figure 1a do indeed reflect the time since U addition. Another way of viewing the concordance of the two systems is to look at the (^{231}Pa/^{235}U) versus (^{230}Th/^{238}U) diagram (Figure 1c). If both Pa and Th are immobile in fluids, the fluid composition should plot next to the origin initially. The composition of fluid once extracted from the slab will evolve along a concordia line [*Cheng et al.*, 1998], and after 60 ka, a mixture of the fluid with a mantle wedge composition plots close to the Tonga lavas. This shows that independent of the normalization to Nb, the constraints given by ^{231}Pa and ^{230}Th systematics are mutually consistent. Clearly, further evidence that both Pa and Th are immobile in fluids would provide an important confirmation of this interpretation (see below). Alternatively, the concordance of the two systems could be coincidental, in which case several more complex processes can be proposed, including addition of Th- and Pa-bearing fluids and in-growth of Pa and Th during melting (see below).

3.3. ^{226}Ra/^{230}Th Systematics

[9] The global surveys of *Gill and Williams* [1990] and *Turner et al.* [2001] have shown that most subduction zone lavas are characterized by ^{226}Ra excesses indicating a recent enrichment of ^{226}Ra relative to ^{230}Th. The ^{226}Ra-^{230}Th fractionation observed in arc lavas is unlikely to be related to a crustal process (plagioclase involvement, interaction with alkali-rich shallow fluids) as in several arcs, (^{226}Ra/^{230}Th) is positively correlated with (^{238}U/^{230}Th). This latter ratio will not be affected by interaction or addition of plagioclase which cannot fractionate U/Th ratios. Similarly, if the ^{226}Ra-^{230}Th fractionation is created by seawater or hydrothermal alteration then (^{234}U/^{238}U) should also be affected. All the observations in arc lavas suggest that shallow level fluids have not modified (^{234}U/^{238}U) ratios.

[10] Ra is an alkali earth and is thus fluid-mobile element unlike Th and Pa, and so fluid addition should result in both ^{238}U and ^{226}Ra excesses over ^{230}Th. However, ^{226}Ra excesses will decay after 8 ka and so a simple, single-stage fluid-addition explanation for the ^{226}Ra-^{230}Th systematics of subduction zone lavas apparently conflicts with the interpretation from the U-Th (and U-Pa in the case of Tonga) arrays that fluid addition of U occurred several tens of kiloannum ago. In a study of U-series disequilibria in Lesser Antilles, *Chabaux et al.* [1999] noted a positive correlation between (^{226}Ra/^{230}Th) and (^{238}U/^{230}Th) ratios which lead these authors to question the time significance of the ^{238}U-^{230}Th arrays and to argue instead that these reflect very recent addition of a fluid that contained not only ^{238}U and ^{226}Ra but also ^{230}Th (in order to explain the sloped ^{238}U-^{230}Th arrays as mixing lines). Thus there appears to be a discrepancy between the ^{226}Ra-^{230}Th systematics and the simplest (U addition only) interpretation of the ^{238}U-^{230}Th, and primarily in the case of Tonga, the ^{235}U-^{231}Pa subduction zone systematics. In an early attempt to reconcile this dilemma, *Turner and Hawkesworth* [1997] suggested that the ^{226}Ra disequilibrium reflects the partial melting process (like the interpretation for ^{235}U-^{231}Pa) and is thus decoupled from the ^{230}Th-^{238}U disequilibria. However, more recent work has established that the magnitude of ^{226}Ra-^{230}Th fractionation in many subduction zone lavas (1–6) far exceeds that observed in most MORB (1–3 and up to 4.2 for one sample) and OIB (typically 1–2), and that (^{226}Ra/^{230}Th) correlates with Ba/Th (Figure 1c) which is an index of slab fluid involvement [*Turner et al.*, 2001]. Ba/Th ratios in MORB and OIB range from 50 to 200 whereas they range between 200 and 1200 in subduction lavas. Both Ba and Th are very incompatible and so are difficult to fractionate during melting of lherzolite for degrees of melting greater than 1%. If the Ba/Th fractionation is produced by the same process as (^{226}Ra/^{230}Th) fractionation, then (^{226}Ra/^{230}Th) must be produced at the base of the melting region where slab fluids are introduced. Another important observation is that (^{226}Ra/^{230}Th) correlates positively with Sr/Th for both the Kamchatka and Tonga-Kermadec lavas (not shown). As Sr is more compatible than Th during melting for all mantle mineralogies, the positive correlation cannot be explained by melting. Rather, it suggests that the relative partitioning of Th and Sr must be reversed and the most obvious explanation is that the larger (^{226}Ra/^{230}Th) and Sr/Th ratios are due to addition of Sr- and Ra-bearing fluids. This last argument removes the ambiguity of the argument with Ba/Th for which the slope of the arrays for melting and slab fluid addition are both positive. Thus while partial melting may enhance ^{226}Ra-^{230}Th disequilibria, it is unlikely to be the main cause of the large (^{226}Ra/^{230}Th) ratios in subduction zone lavas.

3.4. Key Issues

[11] The key objective of this investigation is to arrive at an internally consistent model which can account for the observations in all three U-series systems. There seems little alternative to the interpretation that, at least some of, the observed ^{231}Pa excesses reflect the effects of partial melting. Therefore the competing interpretations and their implications and/or problems for the U-Th and Ra-Th data are as follows:

[12] (1) Interpretation. Neither Th nor Pa is mobilized in subduction zone fluids in which case the U-Th and Tonga U-Pa arrays reflect the time since U addition. Implication. The Ra-Th data reflect addition of Ra by fluids several tens of thousands of years after addition of U either by continuous, or a discrete, late fluid addition.

[13] (2) Interpretation. The Ra-Th data reflect fluid addition less than a 1000 years ago and therefore both Th and Pa are sufficiently mobilized in subduction zone fluids that the U-Th and Tonga U-Pa arrays have no time significance at all. Implication. The coincidence of the U-Th and Pa-Th ages from Tonga are fortuitous.

[14] (3) Interpretation. Fluid addition occurred less that a few kiloannum ago to produce the Ra-Th disequilibria, a horizontal array on the U-Th equiline diagram, and a positive array on the (^{230}Th/^{238}U) versus (^{231}Pa/^{235}U) diagram from which the lavas evolved upward to higher ^{230}Th and ^{231}Pa via the effects of partial melting. Implication. If the ^{235}U excesses in Tonga reflect a lack of U-Pa fractionation during partial melting and if Th is not mobile in fluids, then the U-Th array should be horizontal instead of inclined

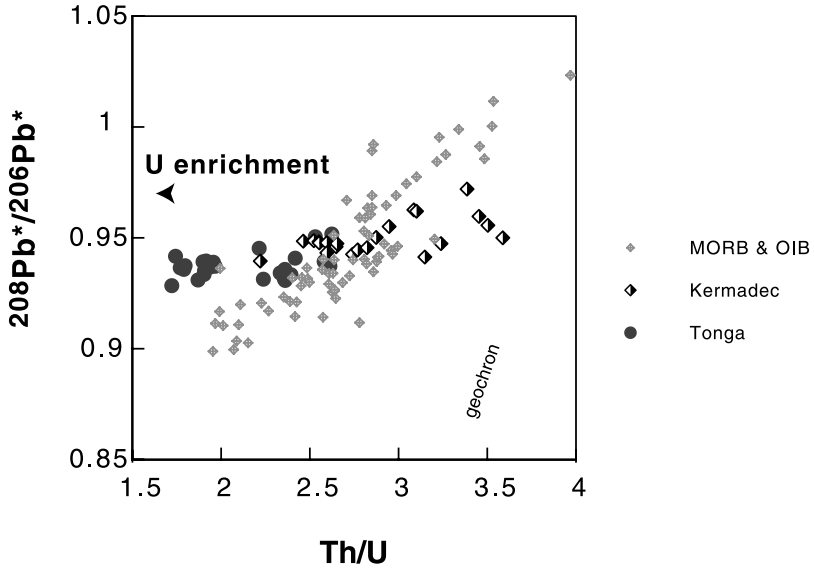

Figure 2. $^{208}Pb^*/^{206}Pb^*$ versus Th/U for Tonga (solid circles) and Kermadec (half-filled diamonds) arc lavas. $^{208}Pb^*/^{206}Pb^*$ are calculated based on Pb isotope composition of the lavas as follows: $^{208}Pb^*/^{206}Pb^* = (^{208}Pb/^{204}Pb_E - {}^{208}Pb/^{204}Pb_{CD})/(^{206}Pb/^{204}Pb_E - {}^{206}Pb/^{204}Pb_{CD})$, where E and CD denote sample and Canyon Diablo (reference for initial Pb composition in the Earth). Th/Us represents the Th/U ratio in the mantle source of the lavas (see text for explanation). Data for MORB and OIB are shown for reference (solid diamonds). This figure shows that Th/U in the source of Tonga lavas has been recently enriched in U while the source of Kermadec lavas has experienced less fractionation as it falls within the mantle array defined by MORB and OIB. Some samples from Kermadec plot to the right of the OIB and MORB array which could reflect mixing with sediments. Even when ($^{230}Th/^{232}Th$) in the Tonga lavas is used to derive Th/U, the Tonga lavas do not plot on the mantle array. This shows that the higher ($^{230}Th/^{232}Th$) in Tonga lavas relative to Kermadec lavas must result from radioactive decay (see text). Tonga-Kermadec data from *Turner et al.* [1997a, 1997b], MORB and OIB data from *Allègre et al.* [1986], *Bourdon et al.* [1996], *Turner et al.* [1997a, 1997b], *Claude-Ivanaj et al.* [1998], and *Dosso et al.* [1999]. The uncertainties in both axes are smaller than the symbol size and cannot explain the dispersion of the arrays.

because ^{238}U-^{230}Th is generally less fractionated during melting than ^{235}U-^{231}Pa.

4. The Validity of U-Th Isochrons in Subduction Zone Magmas

[15] In light of the preceding discussion, it seems to us that the most critical issue at this stage is to try to constrain the interpretation of the inclined $^{238}U/^{230}Th$ arrays because only once this is resolved can the combined U-series isotope data be used to develop a consistent model for fluid addition and partial melting at subduction zones. We now discuss two independent avenues of thought which suggest that the $^{238}U/^{230}Th$ arrays do indeed have time significance.

4.1. The U-Th Fractionation in Subduction Zones Was Recent

[16] Many authors have emphasized that global U-Pb-U-Th and Th-Sr isotope systematics require that there has been a recent U-Th fractionation in subduction zone lavas. ^{208}Pb-^{206}Pb isotope systematics which record the long-term evolution of ^{238}U and ^{232}Th systematics can be used to estimate the time-integrated Th/U ratio of the source. In a $^{208}Pb^*/^{206}Pb^*$ versus Th-U diagram (Figure 2), subduction zone lavas do not fall on the mantle array defined by OIB and MORB [*Allègre et al.*, 1986; *Gill and Williams*, 1990; *McDermott and Hawkesworth*, 1991] and require recent addition of U because this diagram represents the ratio of radiogenic Pb which should be directly related to the ingrowth of ^{208}Pb and ^{206}Pb by decay of ^{232}Th and ^{238}U. If the Th-U systematics of the Tonga-Kermadec arc were to be explained by addition of U-rich fluid to variably enriched mantle characterized by a range in Th/U ratios [e.g., *Elliott et al.*, 1997], this should be detectable on the $^{208}Pb^*/^{206}Pb^*$ versus Th/U diagram. It has been shown that OIB and MORB fall on an array that define the composition of the mantle prior to any recent modification in U-Th-Pb systematics due to melting, or fluid addition (<100 Ma). However, the Tonga-Kermadec lavas form an array that is oblique to the mantle array with the Tonga lavas characterized by low Th/U ratios (Figure 2). There are two possible explanations why the Tonga-Kermadec lavas do not plot on the mantle array: (1) addition of a sediment melt caused recent Th/U fractionation and (2) addition of a U-rich fluid decreased the Th/U ratios. Based on Nd isotopes, it was shown that the source of Kermadec lavas contained a larger sediment contribution than the source of the Tongan lavas [*Turner et al.*, 1997a, 1997b]. Yet these fall on the mantle array or to its right (Figure 2). The sediments subducted beneath Tonga and Kermadec contain a large amount of Pb with a very distinct isotope composition compared with the upper mantle. Therefore addition of sediment to the mantle wedge will result in a

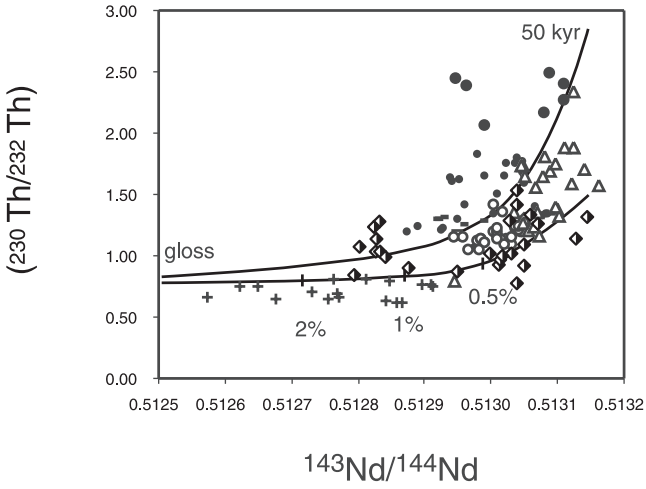

Figure 3. (^{230}Th/^{232}Th) versus ^{143}Nd/^{144}Nd ratios for arc lavas. This diagram shows that there is a general correlation between (^{230}Th/^{232}Th) and ^{143}Nd/^{144}Nd for the global arc data set. However, when looking at individual localities, there is no clear correlation between (^{230}Th/^{232}Th) and ^{143}Nd/^{144}Nd. This suggests that the (^{230}Th/^{232}Th) ratios do not reflect a long-lived heterogeneity in Th/U ratios. Symbols and data sources are same as in Figure 1, Vanuatu data from *Turner et al.* [1999]. The curves indicate mixing lines between a mantle source and sediment. Mantle source contains 0.011 ppm Th, 0.67 ppm Nd, and 0.004 ppm U, and has ^{143}Nd/^{144}Nd = 0.51315 and (^{230}Th/^{232}Th) = 1.5, to which was added sediment with the composition of GLOSS [*Plank and Langmuir*, 1998], amounts indicated as percentage along the curve. To this combined wedge plus sediment composition a constant U flux of 0.14 ppm was then added and the upper curve indicates the resultant (^{230}Th/^{232}Th) ratios to which this three-component mix would evolve after 50 ka.

variation of ^{208}Pb*/^{206}Pb*. If this addition of sediment also produces a variation in Th/U then ^{208}Pb*/^{206}Pb* should be correlated with Th/U, which is not observed.

[17] Moreover, if the Tonga-Kermadec mantle was characterized by variable Th/U ratios (hence variable (^{230}Th/^{232}Th)) prior to fluid addition, then there should be a correlation between (^{230}Th/^{232}Th) and ^{143}Nd/^{144}Nd ratios (Figure 3) because Nd isotope ratios are mostly sensitive to sedimentary contribution. If a small addition of sediment (<1%) were responsible for the variation in (^{230}Th/^{232}Th), a local correlation with ^{143}Nd/^{144}Nd ratios should be observed. While there is an overall global correlation between these two parameters that reflects mixing between a sediment component and the mantle wedge, there is no within subduction zone correlation (Figure 3).

[18] Conversely, the Tonga lavas display the largest fractionation to the left of the mantle array. Even if the Th/U measured in the lavas were used instead of the Th/U based on ^{230}Th/^{232}Th (but see *Elliott* [1997]), the Tonga samples would still be distinct from the mantle array (not shown). Taken together these observations suggest that the higher (^{230}Th/^{232}Th) in the Tonga lavas relative to Kermadec must result from radioactive decay. The observation from the Kermadec lavas suggests that sediment addition did not perturb the U/Th system enough to displace their source region to the left of the mantle array. If the Th/U fractionation was recent (<10 ka), then the Th/U ratio of the source, estimated from the (^{230}Th/^{232}Th) ratio, should fall on the mantle array. Consequently, this second observation indicates that the displacement of Tonga lavas reflects recent fluid addition rather than an ancient fractionation event.

[19] Overall, this suggests that the U enrichment is recent rather than long-lived and decoupled from the enrichment recorded by Nd isotope ratios. The observations based on Pb and Nd isotopes therefore suggest that the observed ^{238}U-^{230}Th ratios reflect fractionation that is reflected in their (^{230}Th/^{232}Th) ratios but not in long-lived Pb isotope ratios. The implication is that the inclined arrays on the U-Th isochron diagram may have time significance.

4.2. Relative Mobility of U Versus Th

[20] U becomes more mobile than Th when it is hexavalent as in the case of oxidizing fluids derived from the slab. However, if there is some Th in the fluid, as suggested by some experimental studies [*Keppler*, 1996; *Brenan et al.*, 1996], the inclined U-Th isotope arrays could reflect mixing between the mantle wedge and an U-rich fluid containing some Th [*Elliott et al.*, 1997]. In order to investigate the composition of the fluid end-member, the arc data have been plotted in a (^{230}Th/^{238}U) versus (^{232}Th/^{238}U) diagram (Figure 4). If fluid addition occurred less than a few 1000 years before eruption (in order to be consistent with the Ra-Th data) and contained some Th to produce the inclined U-Th arrays, then the fluid end-member should fall on a line going between the origin and the Th/U ratio of the altered oceanic crust. The U/Th ratio of this fluid can then be compared with that predicted from the experimental fluid partition coefficients for U and Th. The model curves shown in Figure 4 are calculated for experimental values of the partition coefficients found in the literature. Based on a compilation of four arcs (Tonga, Kamchatka, Marianas, and Vanuatu) it can be seen, first, that the composition of the fluid has to be different for each arc, and second, that the (^{230}Th/^{238}U) ratio of the putative fluid would have to be as high as 0.6 or even equal to 1 if we take the Kamchatka or Philippine data. This would require that the partition coefficients for U and Th are on the same order of magnitude, which is completely inconsistent with experimental data [*Keppler*, 1996; *Brenan et al.*, 1996] when the oxygen fugacity is appropriate to that inferred for the subarc mantle [*Balhaus et al.*, 1990, *Parkinson and Arculus*, 1999; *Blatter and Carmichael*, 1998]. Thus it would appear that the mobility of Th has to be unrealistically high in subduction fluids to explain the data in that way. The alternative explanation of the arrays in Figure 4 is aging following addition of a fluid containing only U (or some combination of Th mobility and ageing, and/or fractionation during partial melting). A similar approach can be used to assess the mobility of Pa. A plot of (^{231}Pa/^{235}U) versus Nb/U ratios for the Tonga lavas reveals a positive trend (Figure 4). This diagram is equivalent to the Th/U diagram of Figure 4 and the fluid composition can be obtained at Nb/U = 0 which corresponds to (^{231}Pa/^{235}U) ratio of 0.7. Again, this would require that Pa is as mobile as U, which is clearly inconsistent with inferences based on its behavior in aqueous solutions [*Guillaumont et al.*, 1968] as Pa shows strong

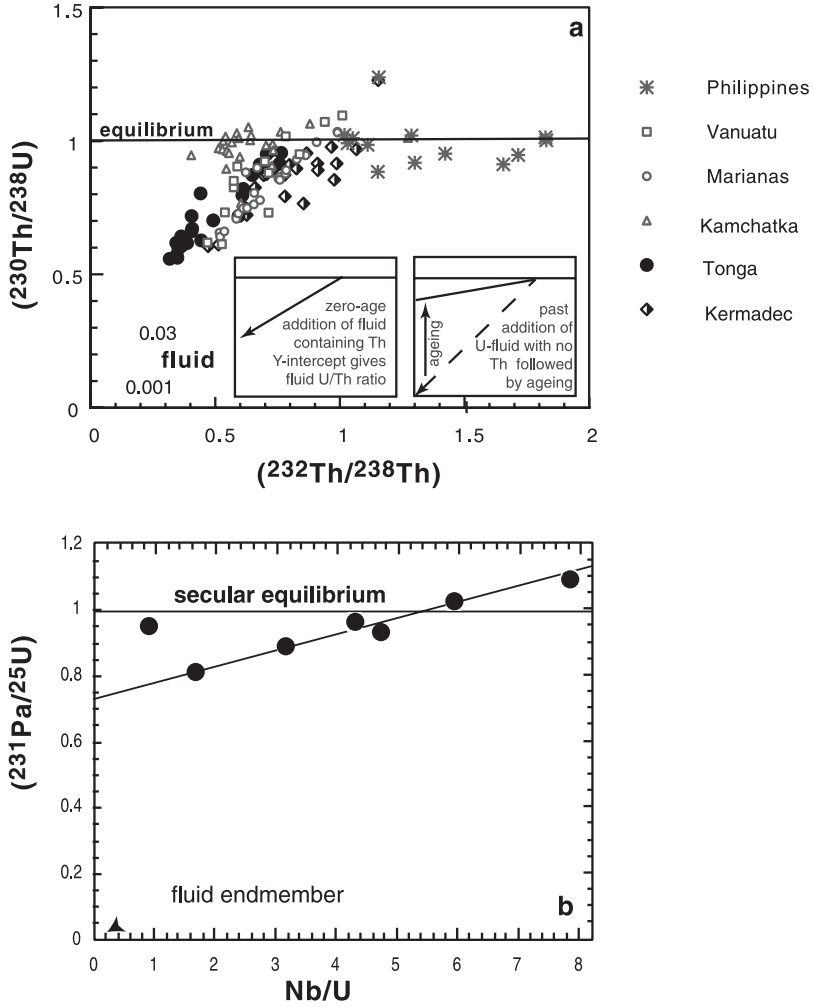

Figure 4. (a) Compilation of mass spectrometry measurements of Th-U disequilibria in arc lavas plotted in a (^{230}Th/^{238}U) versus (^{232}Th/^{238}U) diagram. In this representation, the fluid end-member should plot on a 1:1 line consistent with experimental partition coefficients between mineral and fluid [*Keppler*, 1996]. The loci of fluid composition based on a batch model for fluid release are shown as a solid line. There is no unique mixing line between a fluid end-member and an end-member closer to the equiline (see text for explanations). Symbols and data sources are same as in Figure 1. The partition coefficients between fluid and mineral are 0.02 and 0.2 for Th and U, respectively, and the amount of fluid released ranges between 0.1 and 2%. (b) Mass spectrometry of Pa-U data for the Tonga lavas plotted in a (^{231}Pa/^{235}U) versus Nb/U ratio. This figure includes a new determination of Nb contents for sample 26837 5 (T. Plank, personal communication). By assuming that Nb/U = 0 in the fluid component, a (^{231}Pa/^{235}U) of 0.7 can be estimated. This high ratio most likely reflects in-growth of ^{231}Pa following fluid addition.

affinities with Nb and Ta. In conclusion, the inclined U-Th and U-Pa arrays would appear to have time significance because their interpretation as the result of mixing with a fluid containing Th and Pa requires unrealistically high fluid partition coefficients for Th and Pa. The corollary is that that there must be a decoupling between Ra-Th and Th-U disequilibria.

5. Constraints on the Mechanisms of Dehydration and Melting

5.1. Possible Dehydration Models

[21] The simplest interpretation of the subduction zone data would be the one in which the fractionation of all of the U-series nuclides occurred during a single fluid dehydration/melting event. However, the observations discussed above appear to favor a model where addition of U by fluids occurs over a timescale comparable to the ^{230}Th and ^{231}Pa half-lives. Therefore the production ^{226}Ra-^{230}Th disequilibrium is likely to be decoupled from U-Th and U-Pa. Since melting appears to be ruled out as the principle cause of ^{226}Ra-^{230}Th fractionation, the excess ^{226}Ra would appear to be derived from fluid addition [*Turner et al.*, 2000, 2001]. This interpretation is not straightforward because it requires "at least" two dehydration events [*Turner et al.*, 2000]. One possibility is that dehydration is continuous and takes place over a timescale that is significant with respect to the half-life of ^{230}Th. An attraction of this model is that it would be

consistent with the experimental evidence that metamorphic dehydration reactions are not restricted to discrete events within the downgoing slab [*Schmidt and Poli*, 1998]. This possibility was considered initially by *Dosseto and Bourdon* [2000] for modeling the Kamchatka data set. Using the fluid partition coefficient determined by *Keppler* [1996], it was shown that the Kamchatka data set could not be reproduced by a continuous dehydration model. This constraint might be relaxed if a different mineral/fluid partition coefficient for U is used [*Dosseto et al.*, 2003]. This type of model is further considered in the next section which discusses various melting models.

[22] Irrespective of whether the process of dehydration is ultimately determined to be continuous or discrete, the U-series evidence (and particularly the elevated (^{230}Th/^{232}Th) observed in some arc lavas such as the Kamchatka arc) is that fluid addition takes place over a time span of several tens of kiloannum. In practice, dehydration probably occurs over an even longer time period as suggested by the petrological experiments [*Schmidt and Poli*, 1998], but the U-series signal that can be preserved in subduction zone rocks represents a time window in this longer process because not all the fluid released necessarily results in subaerial volcanic activity.

5.2. Models for Partial Melting at Subduction Zones

[23] Many models have been developed to explain U-series fractionation in mid-ocean ridge and ocean island basalts. Partial melting beneath both mid-ocean ridges and ocean islands occurs in response to adiabatic decompression and what differs between the various models are the partition coefficients [*Beattie*, 1993; *Lundstrom et al.*, 1994; *Landwehr et al.*, 2001], the relative fraction of melt to matrix (porosity), the melt productivity, the extraction rates of melt from a porous matrix [*Williams and Gill*, 1989; *Iwamori*, 1994], the degree of equilibration of the melt with the matrix [*Spiegelman and Elliott*, 1993; *Iwamori*, 1994; *Qin*, 1992], and the porosity structure [*Iwamori*, 1994; *Lundstrom*, 2000]. A key point of this paper is that these models are not directly applicable to subduction zone magma generation because melting is, at least promoted, by fluid addition and there is no a priori requirement for adiabatic decompression of the mantle wedge. Nevertheless, a component of decompression melting has been inferred from major and trace element data which suggest that the degree of melting in subduction zone lavas depends on the thickness of the crust beneath subduction zone volcanoes [*Plank and Langmuir*, 1988]. However, it has also been argued that, in a static mantle, the melt fraction will increase as a hydrous melt ascends through hotter mantle to the subduction zone [*Davies and Bickle*, 1991; *Grove et al.*, 2002] as long as the melts interact with the peridotitic matrix. Thus the inferences from geochemistry for adiabatic upwelling beneath arc volcanoes [*Pearce and Parkinson*, 1993; *Plank and Langmuir*, 1988] should be considered with some caution.

[24] In the case of partial melting and U-series data in subduction zones, there are two key observations that need to be explained. First, the large Ra-Th disequilibria must be produced very deep near the base of the melting column requiring that fluid and melt migration times are extremely fast [*Turner et al.*, 2001]. This is radically different from the chromatographic porous flow model interpretation for mid-ocean ridges where the large Ra excesses are thought to be produced near the top of the melting column [*Spiegelman and Elliott*, 1993]. Second, Pa excesses, which are found in most subduction zone lavas [*Pickett and Murrell*, 1997; *Bourdon et al.*, 1999; *Dosseto and Bourdon*, 2000] must have overprinted any previous effects of U-fluid addition which would result in ^{231}Pa deficits. The only location where ^{231}Pa deficit has been found relative to ^{235}U is in Tonga [*Bourdon et al.*, 1999] which is also characterized by large ^{230}Th deficit relative to ^{238}U. These data would appear to require that the more commonly observed Pa excess are produced subsequent to fluid addition by the melting process.

[25] We now review several of the subduction melting models that have been proposed in the literature bearing in mind that (1) the degree of melting of arc [*Pearce and Parkinson*, 1993; *Plank and Langmuir*, 1988; *Hirschmann et al.*, 1999] is estimated to be similar (or larger) to the degree of melting of mid-ocean ridge tholeiites (5–20%) and (2) the rate of magma production (which is a key parameter for melting models) can be constrained by both the rates of crustal production [*Reymer and Schubert*, 1984] and the material fluxes into subduction zones [*Davies and Bickle*, 1991] which can be converted to melting rates (kilograms of magma produced per cubic meter per year), if the size of the melting region is known.

5.2.1. Flux Melting

[26] Subduction zones are sites where the mantle becomes cooled and so the addition of fluid seems essential for, at least the initiation of, melting beneath arcs. If the addition of fluid is instantaneous, it seems likely that the melt should also be produced "immediately." Thus the most reasonable model for flux melting is the classical batch melting model. However, because the partition coefficients for Pa and U are small, it is very difficult to produce large ^{231}Pa-^{235}U disequilibria for degrees of melting >5%. One might envision a single, unique process of melting that would simultaneously produce all the U-series isotope disequilibria (i.e., U, Pa, and Ra excesses). This was suggested qualitatively by *Regelous et al.* [1997] for the Tonga-Kermadec U-Th systematics and has similarities with the models proposed by *Tatsumi* [1989] involving melting of hydrous peridotite. In their model, *Regelous et al.* [1997] suggest that ^{238}U excesses are generated by amphibole breakdown during melting of metasomatized peridotite. However, for this model to also explain the Tonga-Kermadec Pa-U data, which are characterized by both ^{231}Pa excesses and ^{231}Pa deficits relative to ^{235}U, it would be necessary to fractionate U-Pa in both directions by having D_{Pa}/D_U vary during melting. In principle, this is possible during nonmodal hydrous melting if, for example, U was more incompatible than Pa initially and then became more compatible at a later stage. However, quantitative modeling of this process shows that unless the partition coefficient for Pa in the hydrous phase(s) is extremely large (>0.2), in general, it is not possible to maintain a large U enrichment and yet also produce ^{231}Pa enrichment for larger degrees of melting (see Figure 5).

[27] A more complex model of flux melting assumes that melting takes place as a direct consequence of fluid addition, over a range of depths corresponding to continuous

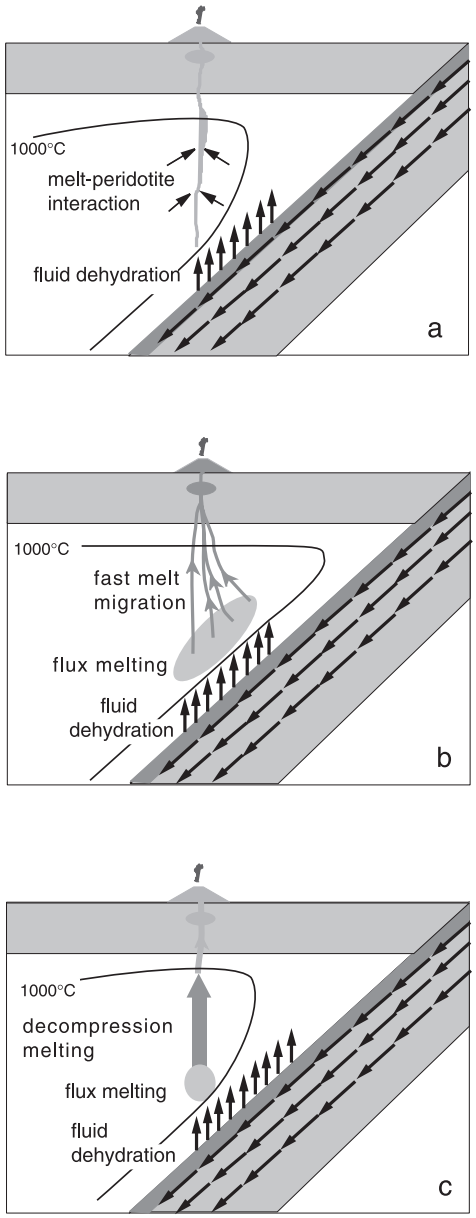

Figure 5. Cartoons of possible models to describe the melting process in subduction zones. (a) Fluid dehydration followed by flux melting and melt-peridotite interaction during ascent. (b) Fluid dehydration immediately followed by flux melting and rapid melt migration over a large range of depths (section 5.2.1). (c) Fluid dehydration followed by flux melting and decompression melting. The model describing adiabatic decompression can be either equilibrium porous flow (see section 5.2.2) or dynamic melting (see section 5.2.3). The diagrams also show expect isotherms corresponding roughly to wet peridotite melting. For the continuous flux melting, the 1000°C isotherm must be almost parallel to the slab, while in the other models, this temperature must be reached at a greater depth.

fluid dehydration. This is an extension of the model proposed by *Dosseto and Bourdon* [2000] and *Thomas et al.* [2001]. It is logical to consider this possibility, as dehydration reactions are likely to proceed over a wide range of pressures as hot isotherms migrate inside the slab and various hydrous phases dehydrate at different pressures [*Schmidt and Poli*, 1998]. The simplest way of modeling this process is to assume repeated episodes of dehydration and melting (Figure 6). Between each episode, both the metasomatized mantle wedge and the dehydrating slab evolve as closed systems. We have assumed that dehydration takes place at a constant rate and that the total mass fraction of water released is 2.5%. In parallel, the metasomatized mantle wedge melts by a fraction F_{max}, which is taken as a variable. The duration of the dehydration/melting process is also taken as a variable. Figure 7 illustrates some solutions for this simple model which shows that it is possible to reproduce the range of U-series disequilibria found in arc lavas for a reasonable set of parameters (see Appendix). As shown in Figure 7c, for short timescales, the Ra-Th and Pa-U are controlled mostly by the fluid contribution. Over longer timescales (up to a few megaannum), as the Ra and U supply from the slab diminish, so do the U and Ra excesses in the integrated melt. In order to produce both ^{231}Pa excesses and ^{238}U deficits in arc lavas, the timescale of the process has to be long enough (>500 ka) to allow ingrowth of ^{231}Pa in the mantle wedge residue. For short

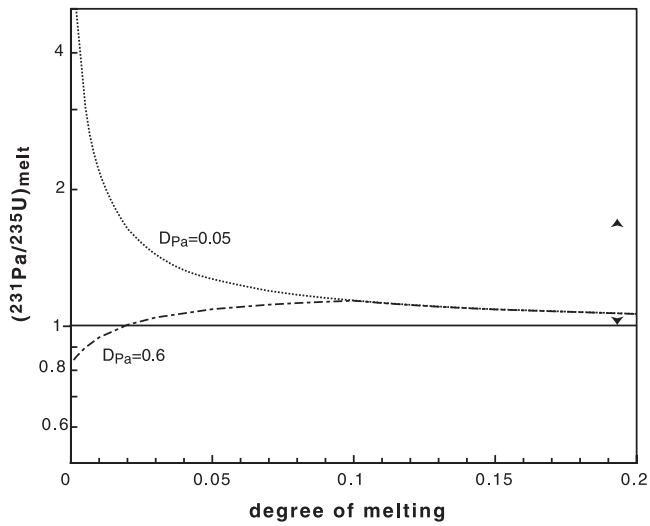

Figure 6. Model curves for ^{231}Pa-^{235}U activity ratios in the melt using a nonmodal melting model with variable partition coefficients during melting to produce both ^{231}Pa excess and ^{231}Pa deficit relative to ^{235}U. This model assumes that U partition into two phases: the phase 1 is characterized by $D_{Pa}/D_U > 1$ ($D_U = 0$) and is consumed during melting ($P = 0.3$) while the other phase is consumed slower ($P = 0.1$) and has $D_{Pa}/D_U << 1$ ($D_U = 0.1$). Two curves are shown to illustrate the sensitivity of the model. The first curve (dashed line) is calculated with $D_{Pa} = 0.6$ in the phase 1 and $D_{Pa} = 0.001$ in the phase 2. The second curve (solid line) is calculated with $D_{Pa} = 0.05$ in the phase 1 and $D_{Pa} = 0$ in the phase 2. This model shows that unless the Pa partition coefficient is extremely large in the first phase, it is not possible to produce both excesses and deficits in activity ratios upon melting. Second, the magnitude in ^{231}Pa excess is far smaller than observed in most arc lavas. The double arrow indicates the approximate range of ^{231}Pa/^{235}U measured in arc lavas.

timescales, the melt signature is dominated by the fluid input. This model shows that it is possible to produce the observed range of U-series disequilibria with a continuous process rather than two discrete steps as proposed by *Turner et al.* [2000] (but see below).

[28] In detail, in order to produce ^{231}Pa excess in the integrated melt, it is necessary to have timescales of melting and dehydration ranging up to several millions of years, if Pa is taken as an immobile element (for example, if D_{Pa} during fluid dehydration is equal to one). On the other hand, if Pa is a fluid-mobile element (but recall the discussion of evidence to the contrary above), then it is possible to generate ^{231}Pa excess ranging up to 100% in the melt for a timescale of several hundreds of kiloannum.

[29] A timescale of several millions of years would correspond to a length scale of hundreds of kilometers for the width of melt generation for a subduction rate of 10 cm a^{-1}, which is clearly excessive. Thus the plausibility of this model relies heavily on undetermined partition coefficients for Pa relative to U and is further discussed in section 5.3.

5.2.2. Decompression Melting: Equilibrium or Disequilibrium?

[30] Decompression melting is the standard model for interpreting U-series data in MORB and OIB [*Spiegelman and Elliott*, 1993; *Lundstrom et al.*, 1995; *Bourdon et al.*, 1996, 1998; *Sims et al.*, 1999]. In the case of subduction zone magmatism, a source of buoyancy (to produce upwelling) as well as decoupling from the downgoing slab motion is necessary in order to facilitate a component of decompression melting. Such increases in buoyancy could result from melting and a local decrease in viscosity due to the presence of fluids in the mantle [*Davies and Stevenson*, 1992]. This is similar to the diapir model for arcs that has been studied both theoretically and experimentally [*Brémont d'Ars et al.*, 1995; *Hall and Kincaid*, 2001]. In the case of diapirs, the assumption of steady state that is generally used to construct melting models is not necessarily verified [*Spiegelman and Elliott*, 1993; *Williams and Gill*, 1989]. Nevertheless, it can be predicted qualitatively that a steady state assumption will necessarily produce a smaller amount of fractionation than melting from a discrete event.

[31] It is possible to produce the observed (^{231}Pa/^{235}U) in subduction zone lavas with the equilibrium porous flow model [*Bourdon et al.*, 1999] as long as the melting rate is slow enough to allow in-growth of ^{231}Pa from ^{235}U as shown in Figure 8. However, if we assume that the mantle wedge source is initially in secular equilibrium in ^{226}Ra-^{230}Th, for

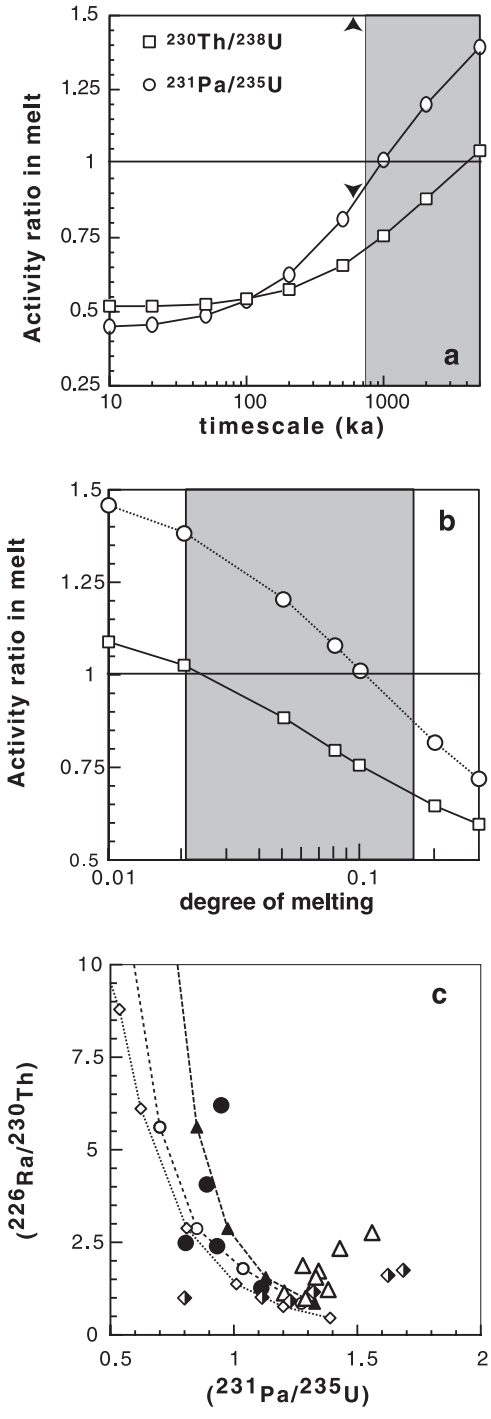

Figure 7. (opposite) Model curves for (^{231}Pa/^{235}U) and (^{230}Th/^{238}U) using the continuous flux melting (model described in Appendix) plotted as a function of (a) timescale of melting and (b) degree of melting (same symbols as in Figure 7a). This model assumes a continuous dehydration and instantaneous melt production and migration. The fraction of melt remaining in the solid matrix is equal to 1‰. Each point represents an aggregated melt composition. The model curves show that it is possible to produce both ^{231}Pa and ^{230}Th excesses or deficits relative to their source depending on the timescale of dehydration and melting and the degree of melting (which scales to a melting rate since the timescale is kept constant in Figure 7b. The boxes indicate the range consistent with observations. (c) (^{226}Ra/^{230}Th) versus (^{231}Pa/^{235}U) diagram showing model curves using the continuous flux melting models. The parameters used for each curve are as follows: diamonds F = 10%, $D^{Pa,f}$ = 1; circles F = 20%, $D^{Pa,f}$ = 0.2; solid triangles F=20%, $D^{Pa,f}$ = 0.05. The timescales of dehydration range from 10 to 5000 ka. The other parameters used in the model are given in Appendix. The double arrow indicates the approximate range of ^{231}Pa/^{235}U measured in arc lavas. Symbols used for data are similar to Figure 1.

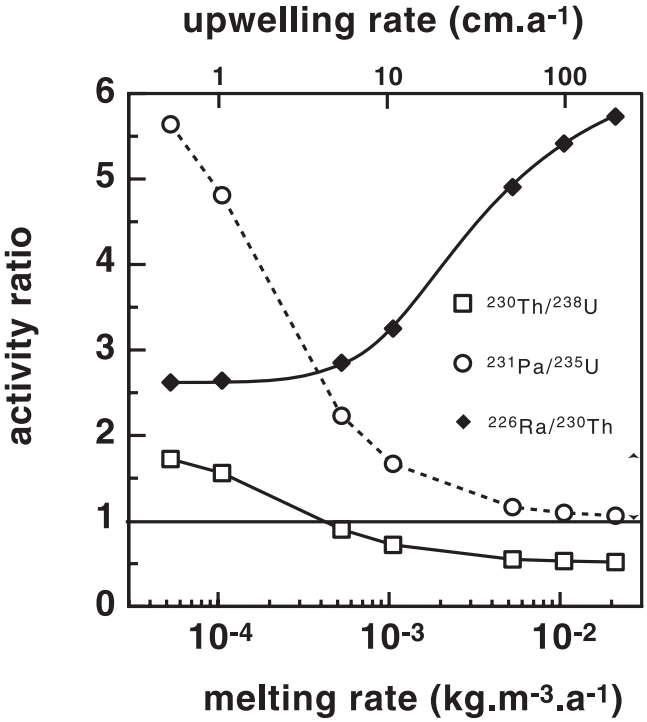

Figure 8. Model curves for the equilibrium porous flow melting model [*Spiegelman*, 2000] showing (^{226}Ra/^{230}Th) and (^{231}Pa/^{235}U) plotted versus melting rate (or upwelling velocity assuming 1% of melting per kilobar of adiabatic decompression). This model assumes initial (^{226}Ra/^{230}Th) = 7 and (^{231}Pa/^{235}U) = 0.8. The matrix porosity is 1‰ and the partition coefficients are D_U = 0.003, D_{Th} = 0.0014, D_{Pa} = 10^{-4}, and D_{Ra} = 10^{-5}. The total degree of melting is 10%. This model shows that the melting rate (and by implication the upwelling velocity) has to be extremely fast (up to 200 cm a^{-1}) in order to preserve the large (^{226}Ra/^{230}Th) produced at the base of the melting column while the corresponding (^{231}Pa/^{235}U) are low. The double arrow indicates the approximate range of ^{231}Pa/^{235}U measured in arc lavas. See text for further explanation.

reasonable sets of parameters, the residence time of ^{226}Ra in the melting column will still be on the order of magnitude of a few 1000 years, which means that the initial excess in ^{226}Ra due to fluid dehydration will have largely decayed and any ^{226}Ra excess will then result from fractionation during melting (Figure 8). It is worth pointing out that a shorter residence for Ra in the melting column (<1000 annum) can only be obtained if the porosity is very low or if the matrix upwelling velocity is greater than a meter per year which does not seem reasonable. Additionally, it will be impossible to produce a correlation between (^{226}Ra/^{230}Th) and Ba/Th (as observed in Figure 1c) with the equilibrium transport melting as shown by *Turner et al.* [2001] since Ba/Th ratio cannot be significantly fractionated during melting, as shown in Figure 1c. For example, in the case of melting of a typical peridotite, Ba/Th ratios would not fractionate by more than a few percent while the observed Ba/Th fractionation in some arc lavas reaches a factor of 25. On the other hand, it is possible to preserve significant ^{226}Ra excess if we assume that the mantle wedge source has been metasomatized with a Ra-bearing fluid. As shown in Figure 8, for melting rates less than 10^{-2} kg m^{-3} a^{-1}, both (^{231}Pa/^{235}U) and (^{226}Ra/^{230}Th) are within the right range observed for the Tonga magmas. However, these melting rates are significantly faster than what has been inferred based on crustal growth rates and petrological models (see below).

[32] Another difficulty in using the equilibrium transport model is that it assumes that melt is always equilibrated with the matrix, which becomes problematic when the melt velocity is large. The question of melt equilibration during ascent can be assessed using a simplified 1-D model used for describing mantle metasomatism by *Bodinier et al.* [1990] and *Hauri* [1997]. The equation describing a process of reactive mass transfer which should be the fastest process allowing reequilibration is:

$$\frac{\partial C_{i,m}}{\partial t'} + \frac{\partial C_{i,m}}{\partial x'} = D_a\left(C_{i,s} - K_i C_{i,m}\right), \tag{1}$$

where D_a is the Damköhler number and K_i is the partition coefficient for element i, and $C_{i,m}$ and $C_{i,s}$ are the concentrations of element i in the melt and the solid matrix, respectively. The Damköhler number is defined as:

$$D_a = \frac{3RL\rho_s(1-\phi)}{w_0 a \rho_m \phi}, \tag{2}$$

where ρ_s and ρ_m are the density of the solid matrix and the melt, respectively (other parameters are defined in caption of Figure 9). By taking the solution at a unit distance δ, one obtains:

$$\frac{C_{i,m} - C_{i,s}/K}{C^0_{i,m} - C^0_{i,s}/K} = e^{-D_a K_i}. \tag{3}$$

With this approach, a simple calculation of the Damköhler number (which is simply the ratio of exchange time to melt migration time) can be used to assess the degree of equilibration of the melt with the matrix, regardless of the process of interaction. Unlike the Peclet number used in the calculation of *Spiegelman and Kenyon* [1992], which does not consider the extent to which reequilibration occurs, the calculation used here takes into account the partition coefficients of the elements considered. Thus the relative abundance of U, Th, and Ra in the melt and the peridotite which controls the extent of reequilibration are taken into account. In contrast to an element like Os, which is very enriched in mantle peridotite relative to the melt, U and Th are enriched in the silicate melt. Thus if the diffusion rates were identical for Os and Th (similar Peclet number), the time necessary for reaching equilibration for Os would be much smaller than for Th (see Figure 9). The parameter that actually controls the degree of reequilibration is D_aK_i which appears in the exponent of equation (3). It can be shown simply that this product is equal to the ratio of the flux of element i being transferred through the mantle by melt advection to the flux of the element i from the solid matrix. Equilibration will be effective if these fluxes have the same order of magnitude. Thus it follows that if $D_aK_i \gg 1$, then the left-hand side of equation (1) is close to 0, which means that there is reequilibration. For $0 < D_aK_I \ll 1$, there is no

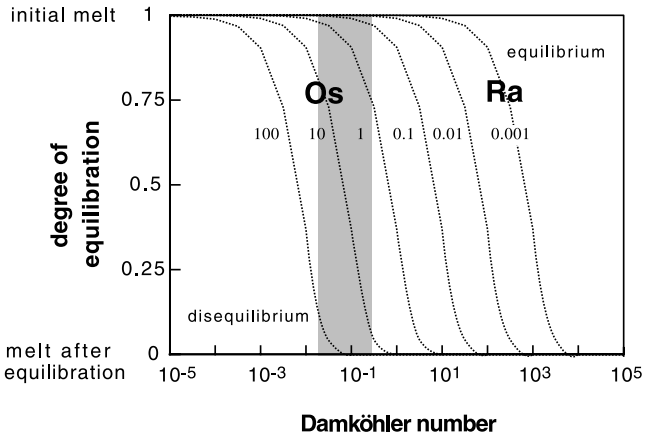

Figure 9. Degree of equilibration versus Damköhler number for a range of solid/melt partition coefficients indicated next to the curves. The Damköhler number is the ratio of the timescale for melt migration relative to the timescale for melt equilibration. Expected Damköhler numbers are marked by a gray box for the case of reactive dissolution. Considering a reactive dissolution rate of 10^{-10} m s^{-1}, both the Os and Ra/Th isotopic systems are expected to be out of equilibrium with a melt velocity of 1000 m a^{-1} (the gray box indicates the corresponding Damköhler number for reactive dissolution). This suggests that radiogenic Os compositions and large (^{226}Ra/^{230}Th) can indeed be derived from a slab signature at the base of a melting column. The parameters used in this calculation are as follows: distance between two channels, d = 1 cm, matrix porosity, 1‰, melt migration distance, L = 50 km. Similar results are obtained with purely diffusive equilibration.

reequilibration since $C_{i,m} = C^0_{i,m}$ If we assume that the melt velocity w_0 is 1 km a^{-1} [*Turner et al.*, 2001], then for channels spaced 1 cm apart, both Os and U (Th) will have D_aK_i which is much smaller than 1 and so there will be no reequilibration (Figure 9). Thus the radiogenic Os signatures, if they can be shown not to be controlled by crustal processes [*Alves et al.*, 1999, 2002; *Borg et al.*, 2000; *Woodland et al.*, 2002], and large Ra-Th disequilibrium [*Turner et al.*, 2001] observed in subduction zone lavas are consistent with a melt transfer rate that is sufficiently fast to prevent reequilibration with the matrix [*Woodland et al.*, 2002; *Turner et al.*, 2001]. The absence of reequilibration required by the fast melt velocity is inconsistent with the basic hypothesis of equilibrium porous flow models which assume melt/matrix reequilibration, throughout the melting column. It is worth noting here that models based on volatile contents and major element data generally suggest high equilibration temperatures for arc lavas (≈1200°C) [*Sisson and Bronto*, 1998; *Grove et al.*, 2002]. These temperatures are much higher than the wet solidus temperature and would suggest that the melts have in fact reequilibrated (at least partially) in the hot core of the mantle wedge on their way to the surface. A possible explanation for the discrepancy between major element evidence and U-series observation is that the solid/melt reequilibration timescales for U-series may be orders of magnitude longer due to more sluggish diffusion of large ions [*Van Orman et al.*, 1998].

[33] Consequently, this analysis suggests that the only model that will satisfy both the Ra and Pa-U disequilibrium data is a model where melt is extracted into a channel and travels rapidly to the surface as we discuss below.

5.2.3. Melt-Peridotite Interaction During Ascent

[34] In this model, we make the assumption that melt is produced above the slab-wedge interface and interacts in the convective mantle wedge with peridotite by crystallizing olivine and partially melting the cooler peridotite. A similar process has been proposed by *Kelemen et al.* [1990] to explain the typical high-field strength element (such as Nb and Ta) depletion in subduction zone lavas and has been investigated by *Bourdon et al.* [1999] for producing U-Pa disequilibrium. In this model, the crystallization of olivine and partial melting of the surrounding matrix does not require full equilibration between incoming melt and matrix. This type of model can potentially be consistent with the Ra-Th disequilibrium data since the melt transport rate can still be extremely fast. The only issue is that, since the mantle wedge is generally very depleted, the degree of melt-peridotite interaction must be extremely large to produce significant fractionation in ^{231}Pa-^{235}U. Similar difficulties were encountered by *Kelemen et al.* [1990] in modeling high-field strength element depletion in arcs by melt-peridotite interaction since the size of the source region with which the magmas need to interact is very large. Alternatively, the mantle wedge material needs to be quite enriched (U_w = 50 ppb, i.e., 2.5 times primitive mantle concentrations) to have a significant leverage during melt-peridotite interaction in order to generate ^{231}Pa excesses that are comparable to the observations as shown in Figure 10. Note that since the degree of interaction could be independent of the initial (^{226}Ra/^{230}Th) activity ratio, there need not be a negative correlation between (^{226}Ra/^{230}Th) and (^{231}Pa/^{235}U) ratios.

[35] To conclude, the results of the modeling show that the mantle wedge needs to be too enriched to reproduce the ^{231}Pa-^{235}U and ^{226}Ra-^{230}Th data. Thus we consider it unsatisfactory to explain U-series systematics in arcs.

5.2.4. Fluid Addition Followed by Dynamic Melting

[36] As shown in the previous section, in order to preserve the large ^{226}Ra excess that is thought to be derived from fluid addition, the melt has to migrate very fast. In the equilibrium porous flow models [*Spiegelman and Elliott*, 1993], such a high melt velocity is inconsistent with the requirement that melts equilibrate all the way to the surface. To obviate this problem, we have considered a dynamic melting model where melt is produced within a porous matrix and then rapidly extracted to the surface via channels with little or no reequilibration.

[37] The velocity through a melt channel can be approximated by a 1-D equation as described by *Turcotte and Phipps Morgan* [1992]. For a 10-cm-wide dike filled with a basaltic magma with a viscosity of 100 Pa s, the melt velocity in a channel can reach 10^{-2} m s^{-1}. The question is of course whether such channels exist in the sublithospheric mantle. The creation of channels is only possible if the fluid/melt pressure exceeds the tensile strength of the matrix [*Stevenson*, 1989]. Given the compaction length of the mantle, the minimum height for a pore-filled melt column necessary to produce a crack is 10 km or a few kilometers depending on the fluid density. Thus this sug-

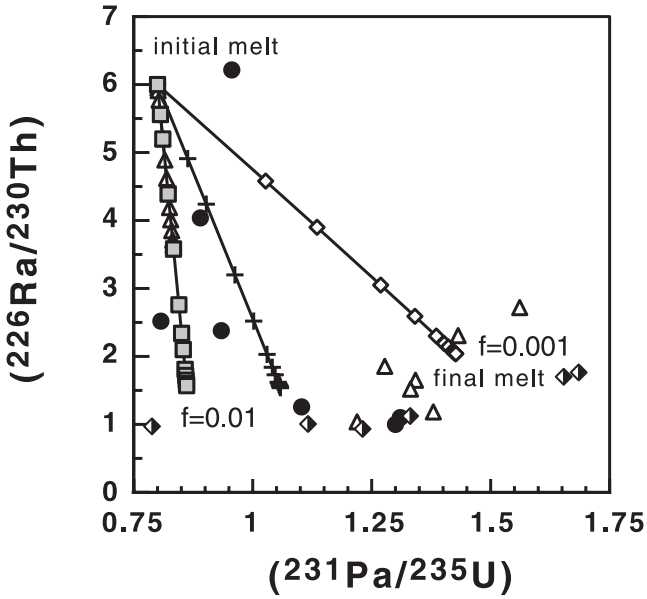

Figure 10. Model curves for (^{226}Ra/^{230}Th) versus (^{231}Pa/^{235}U) during interaction between melt and depleted peridotite using the model by *Bourdon et al.* [1998]. The curves are calculated for variable degrees of melting of the peridotite during interaction (f = 0.01 or f = 0.001) and variable U concentrations in the mantle wedge. Diamonds: U_w = 50 ppb, f = 0.001; triangles: U_w = 5 ppb, f = 0.001; squares: U_w = 5 ppb, f=0.01; crosses: U_w = 50 ppb, f = 0.0025. In all cases, it is difficult to maintain a large (^{226}Ra/^{230}Th) while producing a large enough (^{231}Pa/^{235}U) activity ratio. The other parameters used in this modeling are as follows: ratio of peridotite melt over crystallized melt, r = 0.3, U_{melt} = 0.2, partition coefficients during peridotite melting $D_U = 10^{-3}$, $D_{Pa} = 10^{-4}$, $D_{Ra} = 10^{-5}$. Symbols for data shown here as similar to Figure 1.

gests that the fluid or melt must accumulate in the mantle wedge before hydrofracturing becomes possible. For the fluid flux estimated based on P-T-t models for slab dehydration (0.1–1 kg m^{-2} a^{-1}) [*Peacock*, 1990], the timescale necessary to reach water saturation of a 10-km column ranges between 30 and 300 ka. We are intrigued that this timescale could represent the ages recorded by the U-Th and U-Pa disequilibrium data (see section 4).

[38] There must also be an additional component of melting in order to generate (^{231}Pa/^{235}U) ratios greater than one. In this section, we consider that the additional melt is produced by dynamic melting using the formalism of *Williams and Gill* [1989]. As suggested by *McKenzie* [2000] and *Eggins* [2000], it is possible that melting and melt extraction is not a continuous process. Thus we have also explored the effect of having discrete melting events in the context of dynamic melting (see equations in Appendix). The results of calculations using this model are shown in Figures 11 and 12.

[39] The results of the dynamic melting model show that it is possible to reproduce the observed excesses of ^{231}Pa and ^{226}Ra provided that melt extraction is fast enough to prevent the initial ^{226}Ra excess from decaying in the matrix and the melting rate has to be slow enough to produce ^{231}Pa at the base of the melting column. The periodic melting model is essentially similar to a dynamic melting model except that melting occurs as a series of discrete events. It is possible to produce large enough ^{231}Pa excesses if the melting rate is of the order of 10^{-3}–10^{-4} kg m^{-3} a^{-1} for a porosity of 1‰. This model (like the others) predicts an anticorrelation between (^{231}Pa/^{235}U) and (^{226}Ra/^{230}Th) which is not inconsistent with the available data (Figure 12a).

[40] We have also explored the effect of dynamic melting on ^{230}Th-^{238}U and ^{231}Pa-^{235}U with some distinct initial conditions and the results are reported in Figure 12b. In this modeling, we have assumed the following initial conditions: (1) there is no time lag between fluid dehydration and melting and (2) there is no Th and Pa in the fluids. In the U-Th isochron diagram, the mantle sources must form a horizontal array and (^{231}Pa/^{235}U) is equal to (^{230}Th/^{238}U). As shown in Figure 12b, an important conclusion from this modeling is that it is possible to produce inclined arrays in the U-Th diagram with dynamic melting [*Elliott et al.*, 2001; *George et al.*, 2003]. This stems from the fact that

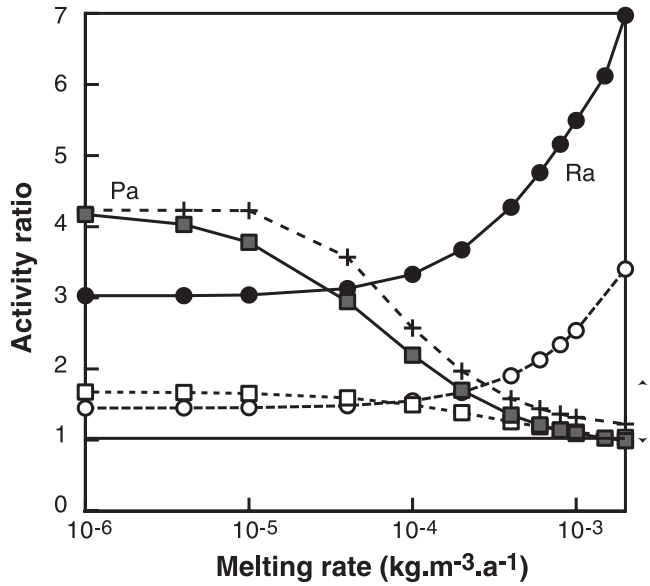

Figure 11. Activity ratios versus melting rate for various dynamic melting models. Solid curves are for a dynamic melting model [*Williams and Gill*, 1989] using a matrix porosity of 0.001. Solid squares (^{231}Pa/^{235}U), solid circles (^{226}Ra/^{230}Th). The open symbols are calculated with the same model with a porosity of 0.005. The crosses represent the (^{231}Pa/^{235}U) activity ratios in the melt with a periodic melting model as described in the text. The initial activity ratio in the source is calculated assuming 2% of fluid with an excess ^{226}Ra added to the mantle wedge. If the melting rate is large there is not enough time to built in ^{231}Pa. On the other hand, if the melting rate is too small, the initial ^{226}Ra excess in the source decays rapidly and the maximum excess ^{226}Ra is three. These calculations show that there must be a trade-off in the melting rate and that it must be on the order of 10^{-3}–10^{-4} kg m^{-3} a^{-1} for the partition coefficient used here (D_{Pa} = 0.0001, D_U = 0.003, D_{Th} = 0.002, $D_{Ra} = 10^{-5}$) to explain the range of (^{231}Pa/^{235}U) and (^{226}Ra/^{230}Th) found in arc lavas (see range shown by double arrow).

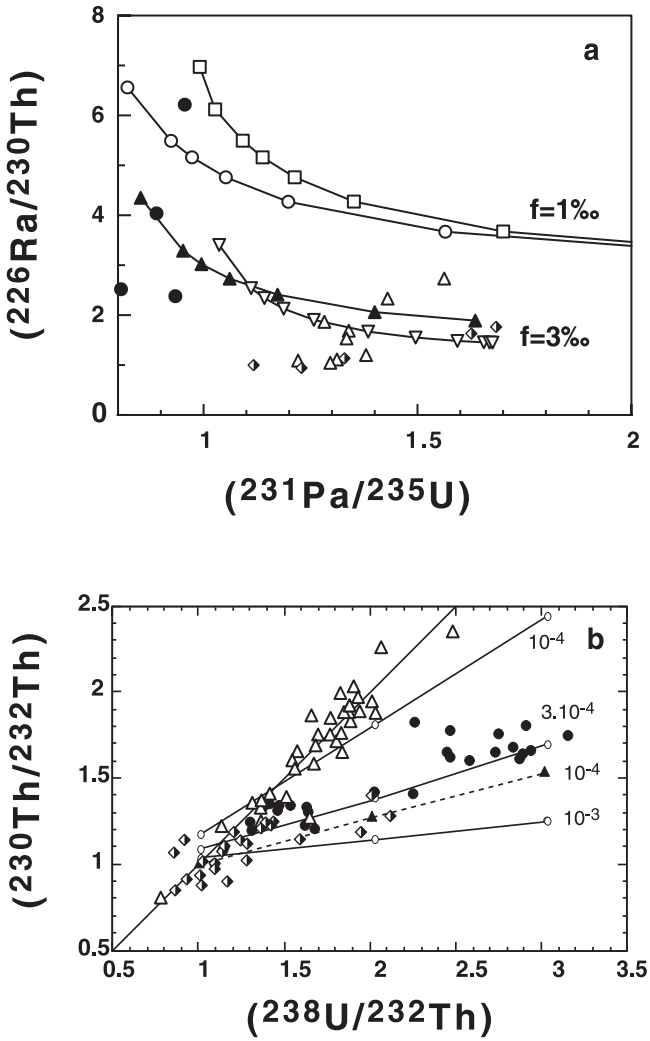

Figure 12. (a) (^{226}Ra/^{230}Th) versus (^{231}Pa/^{235}U) calculated for various melting rates with a dynamic melting model. The model curves are estimated based on initial (^{226}Ra/^{230}Th) = 7 prior to melting. Matrix porosity in permil is indicated next to the curves. The curves with upward triangles and open circles are calculated with an initial (^{231}Pa/^{235}U) = 0.8, simulating a previous addition of fluid to the mantle wedge. The curves with squares and inverted triangles assume an initial (^{231}Pa/^{235}U) = 1 in the mantle wedge source. Solid circles, Tonga-Kermadec data; open squares, Kamchatka data. (b) ^{230}Th-^{238}U disequilibrium calculated for various melting rates and initial conditions with a dynamic melting model plotted in a ^{238}U-^{230}Th isochron diagram [*Elliott*, 2001; *George et al.*, 2003]. The porosities are 10^{-3}. Model curves are labeled with melting rate in kg m^{-3} a^{-1}. The model curve with solid upward triangles correspond to a depleted mantle wedge source with 2% cpx ($D_U = 3 \times 10^{-4}$ and $D_{Th} = 2.6 \times 10^{-4}$). The larger in-growth in (^{230}Th/^{232}Th) are obtained for slower melting rates. The model curves are compared with U-Th data from the Kamchatka and the Tonga-Kermadec arcs [*Bourdon et al.*, 1999; *Turner et al.*, 2000; *Dosseto et al.*, 2003]. Symbols used for plotting the arc data are same as given in Figure 1. The other parameters are the same as those used in Figure 11.

for samples that start off with large ^{238}U excesses, the decay equation predicts a faster increase in (^{230}Th/^{232}Th) than for samples close to the equiline for the same input parameters. This results in inclined arrays in the ^{238}U-^{230}Th isochron diagram (Figure 12b). The ability to reproduce the arrays for the Kamchatka or Tonga-Kermadec data set depends on the partition coefficients that are used during melting. If the mantle has 10–12% cpx (or garnet), then this model can produce both data sets. On the other hand, if the mantle wedge is depleted as is generally thought (low cpx and/or garnet mode) then it is harder to match all the U-series disequilibria, in particular, the Kamchatka data set (Figure 12b).

[41] Our model is aimed at providing an explanation for the U-series observations. It underlines the need for a theoretical framework for melt migration that is consistent with the extremely fast melt velocities derived from Ra-Th data. In contrast, with the equilibrium porous flow model, the melting rate does not need to be extremely fast to preserve the initial ^{226}Ra-^{230}Th derived from fluid addition because Ra is more efficiently stripped from the matrix in dynamic melting models. Thus it is possible to produce significant (^{231}Pa/^{235}U) ratios. The dynamic model in itself is able to reproduce the data with or without a time lag between melting and dehydration. The distinction between the two models depends on the partition coefficients for U and Th during melting and hence the degree of previous depletion. It must also be noted that, provided melting is not instantaneous, dynamic melting could be associated with a decompression melting component or further heating of the wedge during downwelling.

5.3. Comparison of Continuous Flux Melting and Dynamic Melting Models

[42] The two models that seem the most realistic for explaining U-series data in arcs are the continuous flux melting and the dynamic melting following fluid addition model. It is difficult to fully decide which model best explains the U-series data. Because the modeling is very dependent on the mineral/fluid partition coefficients that are used for U, Th, and Pa, choosing between the models might ultimately depend on better determination of fluid-mineral partitioning experiments. At this stage, it is still possible to speculate which model might prevail. If Th and Pa are sufficiently fluid-mobile, and if melt is extracted and migrates at low melt fractions, then the continuous flux melting model is feasible and the timescale between slab dehydration and melt extraction could be short over the whole length of the descending slab.

[43] We now discuss some implications of this model that will need to be explored. As shown in section 5.2.1, an estimate of length scale over which melting takes place in the context of this model depends on the amount of ^{231}Pa that can be in-grown or possibly added from the slab fluid. If the length scale amounts to 100 or 200 km, then the melts need to be focused to the arc front and this focusing will require a significant component of horizontal melt migration. As the main driving force for melt migration is its buoyancy, it is not obvious how such a fast lateral melt migration could be possible. This would, for example, require that the trajectory of melts follows the orientation of cracks toward the arc. There is currently only one model

[*Spiegelman and McKenzie*, 1987] that produces melt focusing beneath the arc but this is based on the assumption of porous matrix flow which is not appropriate for arcs.

[44] This model would also imply that the solidus is reached over a wide range of depths right above the slab where fluids would presumably metasomatize the peridotitic mantle. Thus the solidus for hydrous peridotite would have to be reached in the forearc region well before the volcanic front (Figure 6). These implications will then have to be reconciled with the work of *England* [2001] who suggested that the depth to the Benioff zone is essentially controlled by the temperature of the mantle wedge and not by the pressure as had been argued before. If melting occurred in the forearc region as the continuous flux model would suggest, there should be a much wider zone of active magmatism than observed.

[45] If, on the other hand, there is little mobility of Pa or Th in fluids, the continuous flux-melting model cannot explain the data with reasonable timescale and length scale for the melting process. In this case, dynamic melting following fluid addition is probably more consistent with the observations. In this context and if the mantle wedge is sufficiently enriched to produce U-Th fractionation during melting, the U-series data suggest that there is a time lag between the inception of U addition by dehydration prior to melting. There would be several possible explanations for this time lag: either (1) a critical melt fraction must be reached before melt is extracted, (2) melting is not triggered until there is sufficient fluid to lower the solidus, or (3) hydrated mantle has to reach the required isotherm before melting ensues [*England*, 2001], or (4) fluids can only migrate and reach hotter mantle material at high pressure [*Mibe et al.*, 1999]. Melting might then be enhanced by adiabatic upwelling or further heating of the wedge as it is down-dragged to produce ^{231}Pa excess relative to ^{235}U.

[46] Thermal models taking into account temperature-dependent viscosity, and decoupling between the slab and the wedge due to fluid dehydration suggest that hotter temperature above the slab are reached only below the zone of decoupling [*Furukawa*, 1993]. A consequence of this is that wet peridotite solidus is reached only deeper than the zone where dehydration (i.e., slab/wedge decoupling) takes place. Thus these thermal models are more consistent with a model where fluid dehydration precedes melting with a significant time lag as suggested in the dehydration/dynamic melting model proposed in section 5.2.4. More modeling will be necessary to assess the robustness of the Furukawa model, when complex rheologies are involved.

5.4. Size of the Melting Region: Material Fluxes and Melting Rate Beneath Arcs

[47] A parameter that arises in the melting models (as in any melting model for U-series) is the melting rate which is the amount of melt (kg) produced per cubic meter per year. This parameter largely controls the extent to which ^{231}Pa can in-grow in the matrix over the timescale of melt production both in the case of dynamic and equilibrium porous flow melting models. In the case of mid-ocean ridges, the upwelling velocity of the matrix can be scaled to the spreading rate of ridges [*Iwamori*, 1994], but in subduction zones the rate of magma production is more difficult to evaluate. Additionally, the focusing effects

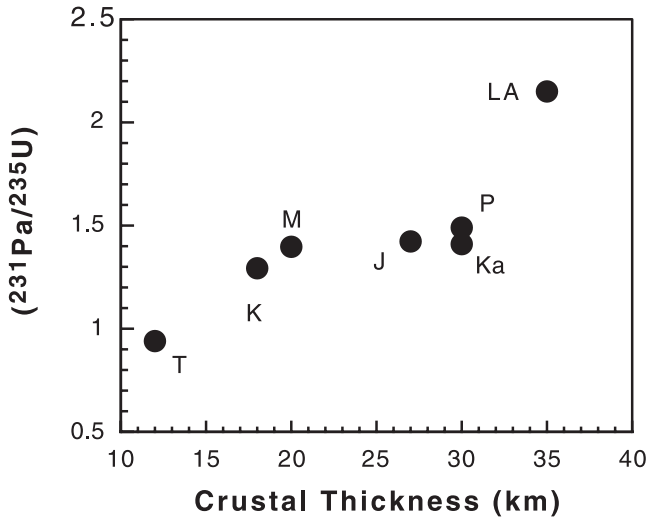

Figure 13. (^{231}Pa/^{235}U) versus crustal thickness for intraoceanic arcs. The positive correlation could be explained by variation in the degree of melting following the model of *Plank and Langmuir* [1988]. An alternative would be that ^{231}Pa/^{235}U activity reflects the melting rate which would be greater when crustal thickness is smaller (corresponding to a thicker overriding plate). ^{231}Pa/^{235}U data are from *Pickett and Murrell* [1997], *Bourdon et al.* [1999], and *Dosseto et al.* [2003]. Crustal thickness data are from *Gill* [1981]. T, Tonga; M, Marianas; K, Kermadec; Ka, Kamchatka; LA, Lesser Antilles; J, Java; and P, Philippines. Only the Tonga, Kermadec, and Kamchatka include more than two samples.

[*Spiegelman and McKenzie*, 1987] that are confined by the lithospheric cap in the case of mid-ocean ridges are less well constrained in subduction zones. Several approaches have been used in the literature. The melting rate derived from the model of *Davies and Bickle* [1991] ranges between 3×10^{-4} and 6×10^{-5} kg m^{-3} a^{-1}using a melting region with a width of 20 km and a height of 50 km. *Reymer and Schubert* [1984] also provide estimates for the melt production integrated over the lifetime of the arc and their numbers compare well with the estimate of *Davies and Bickle* [1991].

[48] As shown by hydrous melting experiments and reemphasized by *Hirschmann et al.* [1999], melt production is likely to depend on the temperature of the mantle wedge. It is predicted that the degree of melting for a given excess temperature above the wet solidus will be a function of the temperature. This means that a hotter mantle wedge should have a higher melting rate. Thermal modeling of the mantle wedge has shown that the mantle should be hotter for a younger overriding plate while an older overriding plate would have the opposite effect [*Kincaid and Selwyn Sacks*, 1997]. This would be consistent with the positive correlation observed between (^{231}Pa/^{235}U) and the thickness of arc crust for intraoceanic arcs (Figure 13). In this context, (^{231}Pa/^{235}U) would be a proxy for the melting rate and the arc crustal thickness would be an indicator of the mantle wedge temperature. Since there is no direct scaling between crustal thickness and mantle wedge temperature, it is not possible to model the correlation shown in Figure 13.

However, it has been shown by *Kincaid and Selwyn Sacks* [1997] that the thickness of the overriding plate has a strong influence on the thermal structure of the mantle wedge. In the case of thick overriding plate the wedge temperature is cooler and the melting rate would be slower. In contrast, a thin overriding plate would result in a hotter wedge and faster melting rates. Modeling of peridotite melting with the program MELTS also predicts greater melt productivity at higher temperatures [*Hirschmann et al.*, 1999].

[49] The range in (^{231}Pa/^{235}U) in the integrated melt can, nevertheless, be explained by melting rates in the range of 2×10^{-4} to 10^{-3} kg m^{-3} a^{-1} using the dynamic melting model developed in section 5.2.3 (Figure 11). This range overlaps with the range found by *Davies and Bickle* [1991] and indicates that the timescale of melt production ($T = \rho_s F/\Gamma$, where Γ is the melting rate) has to be greater than several half-lives of ^{231}Pa (32 ka).

[50] Alternatively, the positive correlation between (^{231}Pa/^{235}U) and the thickness of arc crust for intraoceanic arcs could reflect variation in the total degree of melting, similar to the correlation found between $Ca_{6.0}$ and $Na_{6.0}$ and thickness of arc crust found by *Plank and Langmuir* [1988]. A thicker crust would result imply a shorter melting column with lower degrees of melting which in turn would result in a larger ^{231}Pa-^{235}U fractionation. The two explanations are not necessarily independent of course; they both suggest that the temperature and size of the melting region control ^{231}Pa-^{235}U fractionation.

6. Geodynamical Implications of U-Series Constraints

[51] In this final section, we examine the geodynamical implications that can be derived from the U-series systematics in subduction zones. The process of dehydration that ultimately triggers melting beneath subduction zones must occur approximately beneath the arc such that the mechanism for fluid transfer is rapid and probably vertical. This precludes the process of dehydration advocated by *Davies and Stevenson* [1992] where the net transfer of fluid by a series of dehydration reactions followed by entrainment in the convective wedge was horizontal [*Turner and Hawkesworth*, 1997]. In order to have fast transfer of fluids, the fluid phase must exist as a free phase which in turn implies a relatively hot wedge. We argue that the depth of melting is intermediate and melting does not take place right above the slab but in the hotter interior of the mantle wedge because temperatures near the slab-wedge interface are probably too cold for melting. This is indicated in particular by the absence of a strong garnet signature (indicative of deep melting) in arc lavas. This inference is consistent with thermal modeling [e.g., *Davies and Stevenson*, 1992; *Peacock*, 1990]and inferences from petrology [*Hirschmann et al.*, 1999]. If Th and Pa are fluid-immobile, a time lag of several tens of kiloannum can be inferred between the first slab dehydration detected in the U-series data and eruption of the magmas. Two hypothesis can be proposed: (1) this time corresponds to the time required for the hydrated peridotite to move to an isotherm corresponding to its solidus temperature by convective down-drag in the mantle wedge, or (2) this time corresponds to the time required to cause hydrofracturing of the mantle wedge. In both cases, the rate-limiting process is the supply of fluids to the wedge by dehydration reactions. This timescale would appear to be strikingly similar along a given subduction zone (e.g., Marianas) which suggests that it must be related to geometry, or the thermal structure of the subduction zone itself. This model is consistent with the thermal structure derived from models assuming temperature-dependent viscosity and slab-wedge decoupling [*Furukawa*, 1993] where the wet solidus is reached roughly vertically beneath the arc.

[52] The U-series data do not demand diapiric upwelling of the peridotite matrix beneath the subduction zone but is not inconsistent with it. The melting rate derived from U-Pa data is consistent with rates of crustal productions derived from global mass balance [*Reymer and Schubert*, 1984] and petrological models [*Davies and Bickle*, 1991]. The range in (^{231}Pa/^{235}U) observed for subduction zones worldwide (Figure 13) may then reflect variations in melting rates with the largest melting rates occurring where mantle wedge temperature is highest.

[53] Melt migration is extremely fast which requires a mechanism for forming high permeability channels [*Aharanov et al.*, 1995], which could of course be transient features, within the asthenospheric mantle. This contrasts with mid-ocean ridges where it has been argued that the rate of magma production may be too small to cause hydrofracturing [*Lundstrom*, 2001].

Appendix A

A1. Description of Flux-Melting Model

[54] This model is based on mass balance equations for both the mantle wedge and the slab. We assume secular equilibrium in the U-series decay chain initially. Between two time steps, a fraction of fluid *df* is added to the mantle wedge. The time step between two melt extractions is Δt. The partition coefficients controlling the fluid-mineral fractionation are taken from *Keppler* [1996] and the mineral modes in the dehydrating slab are clinopyroxene, 45; garnet, 45; and olivine, 10.

[55] The initial U concentration in the mantle wedge (U_w) is set to an arbitrary value of unity and all the other nuclides are scaled relative to U_w. The U concentration in the oceanic crust is twice the concentration of the mantle wedge. The Th/U ratio of the mantle wedge and the slab are both equal to 2.5. This value is relevant for modeling the higher (^{230}Th/^{232}Th) observed in some arc lavas.

[56] The model operates with a series of time steps. At each step, a fraction of fluid *df* is added to the mantle wedge. The bulk partition coefficients used for fluid dehydration are $D^{Th} = 0.2$, $D^{U} = 2 \times 10^{-2}$, $D^{Ra} = 7 \times 10^{-4}$, and D^{Pa} is a free parameter; these parameters were estimated as explained by *Bourdon et al.* [2000]. Following this, the metasomatized mantle melts by *dfm* and the partition coefficients used during melting are $D_U = 0.003$, $D_{Th} = 0.0014$, $D_{Pa} = 1 \times 10^{-4}$, and $D_{Ra} = 1 \times 10^{-4}$ which are close to the values used by *Lundstrom* [1995]. We assume that a constant mass fraction f_r remains in the mantle wedge after melt extraction. The bulk composition of the mantle wedge after melt extraction is calculated with the following equation after each extraction:

$$C_R^T = (D(1 - f_r) + f_r)C_m,$$

where C_R^T and C_m represent the concentration in the matrix after melt extraction and in the melt, respectively. Between each time step, both the metasomatized mantle wedge and the slab are assumed to behave as closed system, and simple decay equations are used to track the abundances of U-series nuclides. Figure 6 shows a cartoon of the model.

A2. Analytical Solutions for Periodic Melting

[57] This model assumes that there are several melting episodes with a period of T. The extent of melting at each step is defined as ΔF:

$$\Delta F = \frac{\rho_m \phi}{\rho_m \phi + \rho_s (1 - \phi)},$$

where ρ_m and ρ_s are the density of the melt and solid matrix, respectively. The melting rate is defined as:

$$\Gamma = \frac{\rho_m \phi}{T}.$$

For the first melting step, the activity ratio in the melt can be estimated with a simple batch melting equation:

$$r_1 = r_0 \left[\frac{D_{\mathrm{U}} + \Delta F(1 - D_{\mathrm{U}})}{D_{\mathrm{Th}} + \Delta F(1 - D_{\mathrm{Th}})} \right].$$

The next melting step takes place after T and the activity ratio in the residue can be defined as:

$$r_1^r = \frac{D_{\mathrm{Th}}}{D_{\mathrm{U}}} r_1 \mathrm{e}^{-\lambda T} + 1 - \mathrm{e}^{-\lambda T}.$$

After n melting steps, the activity ratio in the melt is given by the following equation:

$$r_n = 1 + (K - 1) \sum_{i=1}^{n} K^{i-1} \mathrm{e}^{-i\lambda T}.$$

It follows that r_n can be rewritten as:

$$r_n = 1 + (K - 1)\mathrm{e}^{-\lambda T} \frac{1 - K^n \mathrm{e}^{-\lambda n T}}{1 - K\mathrm{e}^{-\lambda T}},$$

where

$$K = \frac{D_{\mathrm{Th}}}{D_{\mathrm{U}}} \frac{D_{\mathrm{U}} + \Delta F(1 - D_{\mathrm{U}})}{D_{\mathrm{Th}} + \Delta F(1 - D_{\mathrm{Th}})}.$$

[58] **Acknowledgments.** We would like to thank Matthew Jull, Peter Kelemen, Stan Hart, Marc Hirschmann, François Chabaux, Max Schmidt, Tim Elliott, Chris Hawkesworth, Jim Gill, and Claude Allègre for discussions. During the writing of this manuscript, we became aware that a model with some similarities was being developed independently by *Thomas et al.* [2002] and we are grateful to them for useful discussions and for sharing a copy of their submitted manuscript. We would like to thank the reviewers for their insightful comments which have helped improve this manuscript.

References

Aharonov, E., J. A. Whitehead, P. B. Kelemen, and M. Spiegelman, Channeling instability of upwelling melt in the mantle, *J. Geophys. Res.*, *100*, 20,433–20,450, 1995.

Allègre, C. J., and M. Condomines, Basalt genesis and mantle structure studied through Th-isotopic geochemistry, *Nature*, *299*, 21–24, 1982.

Allègre, C. J., B. Dupré, and E. Lewin, Thorium/uranium ratio of the Earth, *Chem. Geol.*, *56*, 219–227, 1986.

Alves, S., P. Schiano, and C. J. Allègre, Re-Os isotopic investigation of Java subduction zone lavas, *Earth Planet. Sci. Lett.*, *168*, 65–77, 1999.

Alves, S., P. Schiano, F. Capmas, and C. J. Allègre, Osmium isotope binary mixing arrays in arc volcanism, *Earth Planet. Sci. Lett.*, *198*, 355–369, 2002.

Balhaus, C., R. F. Berry, and D. H. Green, Oxygen fugacity controls in the Earth's upper mantle, *Nature*, *348*, 437–440, 1990.

Beattie, P., Uranium-thorium disequilibria and partitioning on melting of garnet peridotite, *Nature*, *363*, 63–65, 1993.

Blatter, D. L., and I. S. E. Carmichael, Hornblende peridotite xenoliths from central Mexico reveal the highly oxidized nature of subarc upper mantle, *Geology*, *26*, 1035–1038, 1998.

Bodinier, J. L., G. Vasseur, J. Vernières, C. Dupuy, and J. Fabriès, Mechanism of mantle metasomatism: Geochemical evidence from the Lherz orogenic peridotite, *J. Petrol.*, *31*, 597–628, 1990.

Borg, L. E., A. D. Brandon, M. A. Clynne, and R. J. Walker, Re-Os systematics of primitive lavas from the Lassen region of the Cascades Arc, *California, Earth Planet. Sci. Lett.*, *177*, 301–317, 2000.

Bourdon, B., C. Langmuir, and A. Zindler, Rigde-hotspot interaction along the mid-Atlantic ridge between 37°30 and 40°30 N: The U-Th disequilibrium evidence, *Earth Planet. Sci. Lett.*, *142*, 175–196, 1996.

Bourdon, B., J.-L. Claude-Ivanaj, and C. Allègre, U-Th-Pa-Ra systematics for the Grande Comore volcanics: Melting processes in an upwelling plume, *Earth Planet. Sci. Lett.*, *164*, 119–133, 1998.

Bourdon, B., S. Turner, and C. Allègre, Melting dynamics beneath the Tonga-Kermadec island arc inferred from ^{231}Pa-^{235}U systematics, *Science*, *286*, 2491–2493, 1999.

Bourdon, B., G. Wörner, and A. Zindler, U-Th evidence for crustal involvement in the petrogenesis of Nevados de Pachayata, Chile, *Contrib. Mineral. Petrol.*, *139*, 458–469, 2000.

Brémont d'Ars, J., C. Jaupart, and R. S. J. Sparks, Distribution of volcanoes in active margins, *J. Geophys. Res.*, *100*, 20,421–20,432, 1995.

Brenan, J. M., H. F. Shaw, F. J. Ryerson, and D. L. Phinney, Mineral-aqueous fluid partitioning of trace elements at 900 °C and 2.0 GPa: Constraints on the trace element chemistry of mantle and deep crustal fluids, *Geochim. Cosmochim. Acta*, *59*, 3331–3350, 1996.

Chabaux, F., C. Hémond, and C. Allègre, ^{238}U-^{230}Th-^{226}Ra disequilibria in the Lesser Antilles arc: Implications for mantle metasomatism, *Chem. Geol.*, *153*, 171–185, 1999.

Cheng, H., L. R. Edwards, M. T. Murrell, and T. M. Benjamin, Uranium-thorium-protactinium dating systematics, Geochim, *Cosmochim. Acta*, *62*, 3437–3452, 1998.

Claude-Ivanaj, C., B. Bourdon, and C. J. Allègre, Ra-Th-Sr isotope systematics in Grande Comore Island: A case study of plume-lithosphere interaction, *Earth Planet. Sci. Lett.*, *164*, 99–117, 1998.

Davies, J. H., and M. J. Bickle, A physical model for the volume and composition of melt produced by hydrous fluxing above subduction zone, *Pilos Trans. R. Soc. London, Ser. A*, *335*, 355–364, 1991.

Davies, J., and H. Stevenson, Physical model of source region of subduction zone volcanics, *J. Geophys. Res.*, *97*, 2037–2070, 1992.

Dosseto, A., and B. Bourdon, Continuous or discrete slab dehydration for explaining the U-series data from Kamchatka (Russia)?, *J. Conf. Abstr.*, *6*, 429, 2000.

Dosseto, A., B. Bourdon, J. L. Joron, and B. Dupré, U-Th-Pa-Ra study of the Kamchatka arc: New constraints on the genesis of arc lavas, *Geochim. Cosmochim. Acta*, in press, 2003.

Dosso, L., H. Bougault, C. H. Langmuir, C. O. Bollinger, and J. Etoubleau, The age and distribution of mantle heterogeneity along the mid-Atlantic Ridge (31–41°N), *Earth Planet. Sci. Lett.*, *170*, 269–286, 1999.

Eggins, S., Rapid melting causes extreme HFSE & REE depletion in IAT, State of the Arc 2000: Processes and timescales, Extended abstracts, *R. Soc. N. Z.*, 62–65, 2000.

Elliott, T., Fractionation of U and Th during mantle melting: A reprise, *Chem. Geol.*, *139*, 165–183, 1997.

Elliott, T., T. Plank, A. Zindler, W. White, and B. Bourdon, Element transport from slab to volcanic front at the Mariana arc, *J. Geophys. Res.*, *102*, 14,991–15,019, 1997.

Elliott, T., A. Heumann, and G. Koetsier, U-series constraints on melting beneath the Marianas, paper presented at the Geological Society of London Meeting: Intra-oceanic Subduction Systems: Tectonic and Magmatic Processes, 2001.

England, P. C., Why are arc volcanoes where they are?, *Eos Trans. AGU*, *82*(47), Fall Meet. Suppl. Abstract T22D-11, 2001.

Furukawa, Y., Depth of the decoupling plate interface and thermal structure under arcs, *J. Geophys. Res.*, *98*, 20,005–20,013, 1993.

George, R., S. Turner, C. Hawkesworth, J. Morris, C. Nye, J. Ryan, and S.-H. Zheng, Melting processes and fluid and sediment transport rates along the Alaska-Aleutian arc from an integrated U-Th-Ra-Be isotope study, *J. Geophys.*, *108*(B5), 2252, doi:10.1029/2002JB001916, 2003.

Gill, J. B., Orogenic andesites and plate tectonics, 390 pp., Springer-Verlag, New York, 1981.

Gill, J. B., and R. W. Williams, Th isotope and U-series studies of subduction-related volcanic rocks, *Geochim. Cosmochim. Acta*, *54*, 1427–1442, 1990.

Gill, J. B., J. D. Morris, and R. W. Johnson, Timescale for producing the geochemical signature of island arc magmas: U-Th-Po and Be-B systematics in Recent Papua New Guinea lavas, *Geochim. Cosmochim. Acta*, *57*, 4269–4283, 1993.

Grove, T. L., S. W. Parman, S. A. Bowring, R. C. Price, and M. B. Baker, The role of an H_2O-rich fluid component in the generation of primitive basaltic andesites and andesites from the Mt. Shasta region, northern California, *Contrib. Mineral. Petrol.*, *142*, 375–396, 2002.

Guillaumont, R., G. Bouissières, and R. Muxart, Chimie du protactinium, I, Solutions aqueuses de Protactinium penta-et tétravalent, *Actinides Rev.*, *1*, 135, 1968.

Hall, P. S., and C. Kincaid, Diapiric flow at subduction zones: A recipe for rapid transport, *Science*, *292*, 2472–2475, 2001.

Hauri, E. H., Melt migration and mantle chromatography, I, Simplified theory and conditions for chemical and isotopic decoupling, *Earth Planet. Sci. Lett.*, *153*, 1–19, 1997.

Hawkesworth, C. J., J. M. Hergt, R. M. Ellam, and F. McDermott, Element fluxes associated with subduction related magmatism, *Philos Trans. R. Soc. London, Ser. A*, *335*, 393–405, 1991.

Hirose, K., and T. Kawamoto, Hydrous partial melting of lherzolite at 1 GPa: The effect of H2O on the genesis of basaltic magmas, *Earth Planet. Sci. Lett.*, *133*, 463–473, 1995.

Hirschmann, M. M., P. D. Asimow, M. S. Ghiorso, and E. M. Stolper, Calculation of peridotite partial from thermodynamic models of minerals and melts, III, Controls on isobaric melt production and the effect of water on melt production, *J. Petrol.*, *40*, 831–851, 1999.

Iwamori, H., ^{238}U-^{230}Th-^{226}Ra and ^{235}U-^{231}Pa disequilibria produced by mantle melting with porous and channel flows, *Earth Planet. Sci. Lett.*, *125*, 1–16, 1994.

Iwamori, H., Transportation of H_2O and melting in subduction zones, *Earth Planet. Sci. Lett.*, *163*, 65–80, 1998.

Kelemen, P. B., K. T. M. Johnson, R. J. Kinzler, and A. J. Irving, High-field strength element depletions in arc basalts due to mantle-magma interaction, *Nature*, *345*, 521–524, 1990.

Keppler, H., Constraints from partitioning experiments on the composition of subduction-zone fluids, *Nature*, *380*, 237–240, 1996.

Kincaid, C., and I. Selwyn Sacks, Thermal and dynamical evolution of the upper mantle in subduction zones, *J. Geophys. Res.*, *102*, 12,295–12,315, 1997.

Landwehr, D., J. Blundy, E. Chamorro-Perez, E. Hill, and B. Wood, U-series disequilibria generated by partial melting of spinel lherzolite, *Earth Planet. Sci. Lett.*, *188*, 329–348, 2001.

Lundstrom, C., Models of U-series disequilibria generation in MORB: The effects of two scales of melt porosity, *Phys. Earth Planet. Inter.*, *121*, 189–204, 2000.

Lundstrom, C. C., H. Shaw, F. Ryerson, D. Phinney, J. Gill, and Q. Williams, Compositional controls on the partitioning of U, Th, Ba, Pb, Sr and Zr between clinopyroxene and haplobasaltic melts; implications for uranium series disequilibria in basalts, *Earth Planet. Sci. Lett.*, *128*, 407–423, 1994.

Lundstrom, C. C., J. Gill, Q. Williams, and M. R. Perfit, Mantle melting and basalt extraction by equilibrium porous flow, *Science*, *270*, 958–961, 1995.

Marsh, B. D., Island arc development: Some observations, experiments, and speculations, *J. Geol.*, *87*, 687–713, 1979.

McDermott, F., and C. Hawkesworth, Th, Pb, and Sr isotope variations in young island arc volcanics and oceanic sediments, *Earth Planet. Sci. Lett.*, *104*, 1–15, 1991.

McKenzie, D., Constraints on melt generation and transport from U-series activity ratios, *Chem. Geol.*, *162*, 81–94, 2000.

Mibe, K., T. Fujii, and A. Yasuda, Control of the location of the volcanic front in island arcs by aqueous fluid connectivity in the mantle wedge, *Nature*, *401*, 259–262, 1999.

Molnar, P., and P. England, Temperatures in zones of steady-state underthrusting of young oceanic lithosphere, *Earth Planet. Sci. Lett.*, *131*, 57–70, 1995.

Parkinson, I. J., and R. J. Arculus, The redox state of subduction zones; insights from arc-peridotites, *Chem. Geol.*, *160*, 409–423, 1999.

Peacock, S. M., Fluid processes in subduction zones, *Science*, *248*, 329–337, 1990.

Peacock, S. M., T. Rushmer, and A. B. Thompson, Partial melting of subducting oceanic crust, *Earth Planet. Sci. Lett.*, *121*, 227–244, 1994.

Pearce, J. A., and I. J. Parkinson, Trace element models for mantle melting: Application to volcanic arc petrogenesis, *Geol. Soc. Spec. Publ.*, *76*, 373–403, 1993.

Pickett, D. A., and M. T. Murrell, Observations of ^{231}Pa/^{235}U disequilibrium in volcanic rocks, *Earth Planet. Sci. Lett.*, *148*, 259–271, 1997.

Plank, T., and C. H. Langmuir, An evaluation of the global variations in the major element chemistry of arc basalts, *Earth Planet. Sci. Lett.*, *90*, 349–370, 1988.

Plank, T., and C. H. Langmuir, The geochemical composition of subducting sediment and its consequences for the crust and mantle, *Chem. Geol.*, *145*, 325–394, 1998.

Qin, Z., Disequilibrium partial melting model and its implications for trace element fractionations during mantle melting, *Earth Planet. Sci. Lett.*, *112*, 75–90, 1992.

Reagan, M. K., J. D. Morris, E. A. Herrstrom, and M. T. Murrell, Uranium series and beryllium isotope evidence for an extended history of subduction modification of the mantle below Nicaragua, *Geochim. Cosmochim. Acta*, *58*, 4199–4212, 1994.

Regelous, M., K. D. Collerson, A. Ewart, and I. J. Wendt, Trace element transport rates in subduction zones: Evidence from Th, Sr and Pb isotope data for Tonga-Kermadec arc lavas, *Earth Planet. Sci. Lett.*, *150*, 291–302, 1997.

Reymer, A., and G. Schubert, Phanerozoic addition rates to the continental crust and crustal growth, *Tectonics*, *3*, 63–77, 1984.

Schmidt, M. W., and S. Poli, Experimentally based water budgets for dehydrating slabs and consequences for arc magma generation, *Earth Planet. Sci. Lett.*, *163*, 361–379, 1998.

Sims, K. W. W., D. J. DePaolo, M. T. Murrell, W. S. Baldridge, S. Goldstein, D. Clague, and M. Jull, Porosity of the melting zone and variations in the solid mantle upwelling rate beneath Hawaii: Inferences from ^{238}U-^{230}Th-^{226}Ra and 235U-^{231}Pa disequilibria, *Geochim. Cosmochim. Acta*, *63*, 4119–4138, 1999.

Sisson, T. W., and S. Bronto, Evidence for pressure release melting beneath magmatic arcs from basalt at Galungung, Indonesia, *Nature*, *391*, 833–886, 1998.

Smith, G. P., D. A. Weins, K. M. Fischer, L. M. Dorman, S. C. Webb, and J. A. Hildebrand, A complex pattern of mantle flow in the Lau backarc, *Science*, *292*, 713–716, 2001.

Spiegelman, M., Usercalc: A web-based uranium series calculator for magma migration problems, *Geochim. Geophys.*, *1*, 1999GC000030, 2000.

Spiegelman, M., and T. Elliott, Consequences of melt transport for uranium series disequilibrium in young lavas, *Earth Planet. Sci. Lett.*, *118*, 1–20, 1993.

Spiegelman, M., and P. Kenyon, The requirements for chemical disequilibrium during magma migration, *Earth Planet. Sci. Lett.*, *109*, 611–620, 1992.

Spiegelman, M., and D. McKenzie, Simple 2-D models for melt extraction at mid-ocean ridges and island arcs, *Earth Planet. Sci. Lett.*, *83*, 137–152, 1987.

Stevenson, D. J., Spontaneous small-scale melt segregation in partial melts undergoing deformation, *Geophys. Res. Lett.*, *16*, 1067–1070, 1989.

Tatsumi, Y., Migration of fluid phases and genesis of basalt magmas in subduction zones, *J. Geophys. Res.*, *94*, 4697–4707, 1989.

Thomas, R. B., M. M. Hirschmann, M. K. Reagan, H. Cheng, and L. R. Edwards, The role of flux-melting on U-series systematics of young lavas rom Costa Rica and Nicaragua, *Eos Trans. AGU*, *82*(47), Fall Meet. Suppl., F1175, 2001.

Thomas, R. B., M. M. Hirschmann, H. Cheng, M. K. Reagan, and R. L. Edwards, (^{231}Pa/^{235}U)-(^{230}Th/^{238}U) of young mafic volcanic rocks from Nicaragua and Costa Rica and the influence of flux melting on U-series systematics of arc lavas, *Geochim. Cosmochim. Acta*, *66*, 4287–4309, 2002.

Turcotte, D. L., and J. Phipps Morgan, The physics of magma migration and mantle flow beneath a mid-ocean ridge, in *Mantle Flow and Melt Migration at Mid-ocean Ridges*, AGU Geophys. Monogr., vol. 71, edited by J. P. Morgan, D. K. Blackman, and J. M. Sinton, pp. 152–185, 1992.

Turner, S., and J. Foden, U, Th and Ra disequilibria, Sr, Nd and Pb isotope and trace element variations in Sunda arc lavas: Predominance of a subducted sediment component, *Contrib. Mineral. Petrol.*, *142*, 43–57, 2001.

Turner, S., and C. Hawkesworth, Constraints on flux rates and mantle dynamics beneath island arcs from Tonga-Kermadec, *Nature*, *389*, 568–573, 1997.

Turner, S., and C. Hawkesworth, Using geochemistry to map mantle flow beneath the Lau Basin, *Geology*, *26*, 1019–1022, 1998.

Turner, S. C., N. Hawkesworth, and R. P. King, U-Th disequilibria and ocean island basalt generation in the Azores, *Chem. Geol.*, *139*, 145–164, 1997a.

Turner, S., C. J. Hawkesworth, N. Rogers, J. Bartlett, T. Worthington, J. Hergt, J. Pearce, and I. Smith, ^{238}U-^{230}Th disequilibria, magma petrogenesis and flux rates beneath the depleted Tonga-Kermadec island arc, *Geochim. Cosmochim. Acta*, *61*, 4855–4884, 1997b.

Turner, S., F. McDermott, C. Hawkesworth, and P. Kepezhinskas, A U-series study of Kamchatka: Constraints on source composition and melting conditions, *Contrib. Mineral. Petrol.*, *133*, 217–234, 1998.

Turner, S. P., D. W. Peate, C. J. Hawkesworth, S. M. Eggins, and A. J. Crawford, Two mantle domains and the time scales of fluid transfer beneath the Vanuatu arc, *Geology*, *27*, 963–966, 1999.

Turner, S., B. Bourdon, C. Hawkesworth, and P. Evans, ^{226}Ra-^{230}Th evidence for multiple dehydration events, rapid melt ascent and the time scales of differentiation beneath the Tonga-Kermadec island arc, *Earth Planet. Sci. Lett.*, *179*, 581–593, 2000.

Turner, S., P. Evans, and C. Hawkesworth, Ultra-fast source-to-surface movement of melt at island arcs from ^{226}Ra-^{230}Th systematics, *Science*, *292*, 1363–1366, 2001.

Van Orman, J. A., T. L. Grove, and N. Shimizu, Uranium and thorium diffusion in diopside, *Earth Planet. Sci. Lett.*, *160*, 505–519, 1998.

Williams, R. W., and J. B. Gill, Effects of partial melting on the uranium decay series, *Geochim. Cosmochim. Acta*, *53*, 1607–1619, 1989.

Woodland, S., J. Pearson, and D. G. Thirlwall, A platinum group element and Re-Os isotope investigation of siderophile element recycling in subduction zones: Comparison of Grenada, Lesser Antilles Arc, and the Izu-Bonin Arc, *J. Petrol.*, *43*, 171–198, 2002.

B. Bourdon and A. Dosseto, Laboratoire de Géochimie et Cosmochimie, IPGP-CNRS UMR 7579, IGP Tour 14–24 3e etage, 4 Place Jussieu, 75252 Paris cedex 05, France. (bourdon@ipgp.jussieu.fr)

S. Turner, Department of Earth Sciences, Wills Memorial Building, University of Bristol, Bristol, BS8 1RJ, UK.